(NASA-TM-85068) EARTH'S MAGNETIC FIELD AS A RADIATOR TO DETECT COSMIC RAY ELECTRONS OF ENERGY GREATER THAN 10 TO THE 12TH POWER eV (NASA) 51 p HC A04/MF A01 CSCL 04A

N83-34495

Unclas
G3/46 36152

NASA

Technical Memorandum 85068

Earth's Magnetic Field as a Radiator to Detect Cosmic Ray Electrons of Energy > 10^{12} eV

S. A. Stephens and
V. K. Balasubrahmanyan

JULY 1983

National Aeronautics and
Space Administration

Goddard Space Flight Center
Greenbelt, Maryland 20771

EARTH'S MAGNETIC FIELD AS A RADIATOR TO DETECT COSMIC RAY ELECTRONS OF ENERGY > 10^{12} eV

S. A. Stephens* and V. K. Balasubrahmanyan

NASA/Goddard Space Flight Center, Greenbelt, MD 20771

* NAS/NRC Senior Research Associate on leave from Tata Institute of Fundamental Research, Bombay, India

ABSTRACT

We have examined in detail the synchrotron emission by electrons of energy greater than a few TeV in Earth's magnetic field. The photon spectrum lies in the X-ray and γ-ray region. As the emission takes place in a narrow cone along the direction of electron, the photons would be incident nearly along a straight line on a detector. This unique feature provides the signature to identify the electron unambiguously. The mean energy of the photons being proportional to the square of the electron energy allows us to determine the energy accurately. Though it may appear that one needs to know the arrival direction of electrons to obtain its energy, we have shown that an omnidirectional detector can be satisfactorily used to estimate the energy. We also show that the collecting power of the detector is a sensitive function of the area of the detector A, the energy of electron E_o, and the number of photons required to identify an electron n_γ; asymptotically the collecting power is proportional to $A^{1.43} E_o n_\gamma^{-1.8}$. An instrument, with a energy threshold for the detection of photons, can be used to measure reliably the integral flux of electrons, even if it has limited energy resolution. We have calculated the event rate expected using an ideal balloon-borne detector capable of detecting above 20 keV at 4 g cm^{-2} of atmospheric depth over Palestine, Texas, and compared with the expected rates using instruments based on currently available technique of detection.

1. INTRODUCTION

High energy cosmic ray electrons play an important role in the understanding of the propagation of cosmic rays. This stems from the fact that, unlike nuclei, electrons have a very low mass and as a result, they suffer severe energy loss especially at high energies through synchrotron radiation and inverse Compton scattering processes. The lifetime of 1 TeV electron against such energy loss processes, in a typical interstellar environment, is about a few times 10^5 years; this lifetime decreases linearly with energy. As a result, the flux of high energy electrons are depleted. The shape of the energy spectrum of electrons at energies beyond a few TeV would be dependent upon the distribution of sources in the solar neighborhood and perhaps on the local dynamics of the propagation of cosmic rays. The influence of a strong nearby source would also be seen as a marked enhancement over the depleted electron spectrum. This information is difficult to obtain from other components of cosmic rays and thus the detection of ultra high energy cosmic ray electrons has profound implications on our understanding of the propagation of cosmic rays in the solar neighborhood.

A variety of experimental techniques has been employed to measure the energy spectrum of cosmic ray electrons below a few hundred GeV (see Balasubrahmanyan and McDonald, 1974). However, beyond this energy only large area nuclear emulsion detectors (Anand, Daniel, and Stephens, 1973; Nishimura et al., 1980) and a large area calorimeter (Muller and Meyer, 1973) have been made use of to extend the energy up to about 1 TeV. The limited collecting power of these detectors does not permit the extension of the electron spectrum beyond 1 TeV. A transition radiation detector, in combination with an ionization calorimeter, placed on the space shuttle (Ormes, 1982) could reliably measure the energy spectrum only to about a few TeV. The limitation,

of this technique, to extend the measurements to higher energies comes from the fact that one needs a deep calorimeter and a transition radiator with sufficiently large spacings between elements (Cherry, 1978). The net results of these modification are to increase the total weight of detectors for the same area and to decrease the available solid angle. Thus, it appears that direct measurement of the energy spectrum of high energy electrons beyond a few TeV seems difficult with the existing techniques.

We have also examined the possibility of detecting cosmic ray electrons by their shower development in the atmosphere; here one cannot distinguish between gamma rays and electrons. For a typical mountain altitude, one can make use of this technique for energies beyond 10^{14} eV. In order to eliminate air showers simulated by nuclear active particles to one part in 10^5, one requires very large area detectors to monitor hadrons and muons associated with a shower. The required area of these detectors is such that the steady hadron and muon flux, resulting from the interaction of cosmic rays at all energies, is sufficiently large enough to be in coincidence with an electron event. As a result, the rare electron air shower would be mistaken for a nucleon initiated cascade and get vetoed. It is quite clear that in spite of the difficulty in making very large area detector arrays, it may not be possible to detect electron initiated showers in the atmosphere.

High energy electrons lose energy through synchrotron radiation in the Earth's magnetic field. An electron of energy 10^{13} eV radiates photons in the energy region between a few keV and a few MeV. These photons are emitted in the direction of the electron within an extremely narrow cone; they are distributed in the plane of curvature of the electron on the convex side of the curvature. As a result, these photons would be incident on a detector along a straight line with very little spread. This pattern provides a unique signature for the identification of the electron. Because of the fact that

identification of such a signature for an electron event does not require the electron to be incident on the detector, the response area of the detector could be larger than the detector area itself. This property provides large collecting power for the detector, which is very necessary when we look for high energy electrons. Further, the mean energy of the emitted photons is proportional to the square of the energy of the electron. As a consequence, the energy estimation becomes reliable even if a detector has low energy resolution for photons. Thus, the detection of high energy electrons using this technique would open up an important window of energy for the study of primary cosmic ray electrons.

In this paper we study in some detail the synchrotron emission by a high energy electron in the geomagnetic field and its dependence upon different arrival directions over Palestine, Texas, where major balloon-borne experiments are being conducted. We discuss how the response of a detector depends upon the arrival direction of electrons, the different criteria one adopts to identify an electron event, the area of the detector, and the energy of the electron. We then make use of an omnidirectional circular detector to examine whether it is possible to determine the energy of an electron without knowing its arrival direction. We are able to demonstrate the reliability of energy estimation using such a detector system. We then make estimates of the collecting power of a detector as a function of the energy of electrons for different detector areas with different selection criteria. Making use of this information we calculate the event rates expected by folding in the energy spectrum of cosmic ray electrons to show the viability of detecting cosmic ray electrons at energies greater than a few TeV. It may be pointed out that the performance of such a detector would have an advantage in the Equatorial region due to a favorable field configuration.

2. SYNCHROTRON RADIATION OF ELECTRONS IN EARTH'S MAGNETIC FIELD

The theory of synchrotron radiation is extensively discussed in the literature, and here we follow the work of Ginzburg and Syrovatskii (1965). We assume in our treatment that the synchrotron results based on classical electrodynamics is valid in the energy region $> 10^{13}$ eV with magnetic field strength of the order of a few tenths of a Gauss. The power radiated by an electron of energy E_0(TeV) in a magnetic field strength B (Gauss) is

$$P(E_0) = 3.77 \times 10^3 \, B_\perp^2 \, E_0^2 \text{ MeV s}^{-1} \qquad (1)$$

where $B_\perp$ is the component of the magnetic field perpendicular to the direction of electron. This radiation is peaked around an energy

$$E_\gamma^m \simeq 1.9 \times 10^{-2} \, B_\perp \, E_0^2 \text{ MeV}. \qquad (2)$$

If one assumes that most of the energy is radiated around this energy, it is clear from equations (1) and (2) that the mean number of photons emitted is proportional to the field strength $B_\perp$ and is independent of the energy of the electron. It is, therefore, essential to look for this radiation in a region of high magnetic field strength. In the case of Earth's magnetic field with a typical field strength of $B_\perp \simeq 0.3$ Gauss, the number of photons emitted per 15 km of the electron trajectory is about 3 photons which is just sufficient to detect the presence of an ultra high energy electron. The energy of the photons emitted by a few TeV electrons is in the X- and γ-ray regime, which can be detected by instruments used for the study of X- and γ-ray astronomy. The spectral shape of photons emitted by an electron can be written as

$$\frac{dN_\gamma(E_\gamma)}{dE_\gamma} = \frac{3.53 \times 10^5}{E_\gamma} \left(\frac{E_\gamma}{E_c}\right) \int_{(E_\gamma/E_c)}^{\infty} K_{5/3}(\chi)d\chi \quad \text{photon/(MeV.s)} \quad (3)$$

where $E_c = 6.56 \times 10^{-2} B_\perp E_0^2$ MeV and $\chi \int_\chi^\infty = K_{5/3}(\chi)d\chi$ gives the spectral distribution of the power emitted by the electron; $K_{5/3}(\chi)$ is the Bessel function of the second kind.

We have shown in Figure 1 the differential and integral spectra of photons emitted by an electron in a magnetic field of strength $B_\perp = 0.4G$ for electron energies 5, 10, and 50 TeV. A common feature that can be noticed from the shapes of the differential spectra is that at low energies, they have a constant slope of -2/3. The spectrum slowly steepens to a slope of -1.0 around E_γ^m and rapidly drops off exponentially beyond E_c. Further one notices that the absolute flux of low energy photons decreases with increasing energy of the electrons (curves B and C). This property is useful in selecting a suitable detector in order that only a small fraction of the total radiated photons is undetected due to detector threshold. This is well demonstrated by the integral spectra (dashed curves) shown in Figure 1. One notices from the dashed curve A that at 5 TeV more than 75 percent of the radiation takes place above 10 keV and only 5 percent above 1 MeV. This implies that 70 percent of the photons emitted are spread over 2 decades in energy and 50 percent over a factor of 25 in the energy scale. It is quite evident from the dashed curves that they are nearly identical, and they appear to be shifted in the energy scale by an amount proportional to the square of the electron energy. This points to the fact that, in order to cover the m decades of electron energy, one needs an instrument capable of detecting photons over $(m^2 + 2)$ decades in energy.

Synchrotron photons are emitted within a narrow cone in the direction of electron. The radiation is polarized, and the angular distributions of

photons along the two principal directions of polarization are different. The angular dependence of photons in the two principal directions of polarization is written as (Ginzburg and Syrovatskii, 1965)

$$n_\gamma^{(1)}(\theta) \propto (1 + \theta^2/\psi^2)^2 \, [K_{2/3}(G_\gamma)]^2 \tag{4a}$$

and

$$n_\gamma^{(2)}(\theta) \propto (\theta/\psi)^2 \, (1 + \theta^2/\psi^2) \, [K_{1/3}(G_\gamma)]^2 \tag{4b}$$

where

$$G_\gamma = \frac{E_\gamma}{2E_c} \, (1 + \theta^2/\psi^2)^{3/2}. \tag{5}$$

In these equations, $\psi = mc^2/E_o$ and K's are the Bessel functions of the second kind with imaginary arguments. The first component represented by equation (4a) is polarized in the direction perpendicular to the projection of the magnetic field on a plane normal to the direction of motion of the electron. The second component represented by equation (4b) is along the projection of the magnetic field. It is clear from these equations that the first component peaks at $\theta = 0$ and drops off at larger values of θ, while the second component does not contribute at $\theta = 0$ but peaks at a finite value of θ. The relative contribution of these two components is dependent upon the photon energy and the magnetic field strength through equation (5) and through the dependence of E_c on $B_\perp$. One may point out that the angle of emission in inversely proportional to the energy of the electron.

In our calculations, we first determine the number of photons in finite energy intervals through equation (3) and then calculate their angular distributions. Therefore, one needs to obtain the normalized angular distributions of the photons for various values of E_γ/E_c. This is obtained by integrating equations (4a) and (4b) as

$$\int_0^{\pi/2} n_\gamma^{(1)}(\theta)d\theta + \int_0^{\pi/2} n_\gamma^{(2)}(\theta)d\theta = 1. \qquad (6)$$

The normalized angular distribution of the radiated photons are shown in Figure 2 as a function of (θ/ψ) for various values of (E_γ/E_c). It is clear from this figure that the angular distribution is a sensitive function of the energy of the photon; the smaller the value of E_γ/E_c, the wider is the distribution. This behavior results from the fact that the second component becomes important (equation 4b) for small values of E_γ, as it is evident from the appearance of a broad peak for $E_\gamma/E_c = 0.05$. Because of the fact that most of the energy radiated is peaked around $E_\gamma/E_c \simeq 0.29$, the wider distributions, which are characteristic of the low energy photon emission, do not contribute to the integral photon distribution. This is demonstrated in Figure 3, in which we have plotted the angular distribution of photons of energy > 20 keV emitted by an electron of energy $E_0 = 10$ TeV in a magnetic field $B_\perp = 0.24$ Gauss. Curve A in Figure 3 is the number of photons of energy > 20 keV emitted per unit radian by an electron over a path length of 10 km as a function of angle from the direction of motion of the electron. In this case, the value of $E_c = 1.57$ MeV and the threshold energy of 20 keV corresponds to $E_\gamma/E_c = 0.013$; the fraction of photons emitted below 20 keV is about 15 percent. One notices that at small values of θ, the angular distribution of all photons resemble the distributions corresponding to large values of E_γ/E_c in Figure 2 and becomes wider as θ increases, due to the contribution from lower energies. The integral photon distribution $N_\gamma(<\theta)$ within a cone angle θ is shown by Curve C in Figure 3. From this curve one infers that 70 percent of the photons of E_γ > 20 keV are emitted within a narrow cone of 0.65×10^{-7} radian. This correspond to a spread of only 1.3 cms on to a detector placed perpendicular to the path of an electron, if the radiation is emitted

from a distance of 100 km. Similarly, 90 percent of the radiation falls within 2.3 cms.

The angular distribution is narrower for higher energy photons. As a result, most of the radiated energy is concentrated in a small cone. We have shown by Curve B the energy flow $\sum E_\gamma(\theta)$ per unit radian as a function of θ. From this curve, one notices that 90 percent of the energy is contained in a narrow cone of 4.5×10^{-8} radian, which corresponds to a spread of 0.9 cm onto a detector kept at a distance of 100 km from the point of emission. The emission cone decreases linearly as the energy of electrons increases. The effect of increasing the magnetic field increases both the number of photons and their energies. Curve A' in Figure 3 shows the angular distribution when the magnetic field is increased by a factor of two (0.48 Gauss). Since E_γ/E_c is unaffected by the increase of the magnetic field, the angular distribution is nearly unaffected. The flattening of the distribution at large θ values result from the inclusion of photons of energy very much lower than E_c because these photons are now above the low energy threshold set at 20 keV.

From the above discussions it is clear that the spread in the photon distribution is small, compared to the required size of the detector, and one can consider the photons to be distributed approximately along a straight line in the detector. This also implies that very high spatial resolution is not needed to detect electrons. However, higher resolution would provide information on the photon density and on the linear spread, both of which can be made use of in the determination of the energy of the electron. The mean energy of the photons emitted by the electron can be calculated using Equation (3), and it is found that

$$\langle E_\gamma \rangle \approx 0.02\ B_\perp\ E_0^2\ \text{MeV} \qquad (7)$$

which is approximately the energy at which the power radiated by the electron is peaked (equation 2). If the detector has a low energy threshold, the mean energy would be larger; high energy cut-off would give a lower value.

3. MOTION OF ELECTRONS IN EARTH'S MAGNETIC FIELD

In this section we discuss the method of tracing the trajectory of cosmic ray electrons in the Earth's magnetic field. We describe briefly the procedure adopted to calculate the synchrotron emission by the electron as it traverses the geomagnetic field. The equation of motion of a charged particle in a magnetic field is given by

$$\frac{d\vec{v}}{dt} = \frac{e}{mc} (\vec{v} \times \vec{B}) \qquad (8)$$

where e, m and $\vec{v}$ are respectively the charge, mass, and velocity of the particle. This equation can be converted to a system of six simultaneous linear differential equations in spherical coordinates (McCraken et al, 1962) so that one can numerically integrate these equations to trace the trajectory. For the magnetic field term $\vec{B}$ in Equation (8), we have made use of the sixth degree simulation of the geomagnetic field with the field coefficients given by Finch and Leaton (1957). This is done in order to take advantage of the computer program of McCraken et al. (1962) to determine the components $(\vec{v} \times \vec{B})$ in the spherical coordinate system using the complex geomagnetic field potential (we thank Dr. M. A. Shea for this information). It may be mentioned here that, at energies of interest here ($> 10^{12}$ eV), the use of different geomagnetic field coefficients would not alter any of the basic conclusions derived in this paper.

We have chosen a typical balloon altitude corresponding to a depth of

4 g cm^{-2} of atmosphere over Palestine, Texas as the initial point on the trajectory of the electron. The detector plane is assumed to be horizontal. Trajectories with different arrival directions (zenith Z and azimuth East of North ϕ) are traced from the detector plane outwards. For this purpose, stepwise integration was carried out similar to the work of Daniel and Stephens (1966). We have shown in Figure 4a an exaggerated view of the trajectory of an electron. In this figure O is the arrival point, B's denote the steps with step length Δs, and A's are the intercepts on the detector plane by tangents B_1A_1, B_2A_2,... at point B's on the trajectory. The wavy lines are indicative of the photons emitted by the electron. These photons intercept the detector within a narrow angle θ. At each step, the following aspects are examined.

a. From the new coordinates, the local vertical height and the angular deviation are obtained.

b. The total magnetic field strength B and its component perpendicular to the direction of electron $B_\perp$ are determined. In our location, the field is directed approximately towards 30° zenith and about 190° azimuth. Using the value of $B_\perp$, the radius of curvature $R_C(S)$ at $S = \sum S-\Delta S/2$, the distance swept by the tangent $\Delta \ell = \tan \{S/R_C(S)\} \times \Delta S/\cos Z$, and $\ell = \sum \Delta \ell$ (see Figure 4a) are calculated. The angular deviation obtained using procedure (a) is checked against $\tan^{-1} \{\Delta s/R_C(s)\}$.

c. The energy spectrum of synchrotron photons is obtained using E_0 and $B_\perp$. The attenuation length of 20 keV photon is about 3 g cm^{-2} of air and this decreases rapidly with decreasing energy. Therefore, we have considered only photons of energy greater than 20 keV in this analysis. The photon spectrum above 20 keV is then corrected for the attenuation in the air between the point of emission and the detector. The matter traversed by the photons is

obtained from the standard atmosphere using the relation $x = \exp\{(48.5-h)/7.54\}$, where x is the atmosphere depth in g cm^{-2} and h is the vertical height in km; this relationship is valid for $x \lesssim 11$ g cm^{-2}. We have made use of the local zenith angle to correct for the slant depth and the absorption cross-sections compiled by Zombeck (1980) to correct for the absorption.

d. The total number of photons received over $\Delta\ell$, the total energy flow, the mean energy $\langle E_\gamma \rangle$, and their angular distribution are calculated. Using these, we obtained the quantities $N_\gamma(< \ell)$ and $E_\gamma(< \ell)$. These are found to be proportional to ℓ^β, where $\beta = 0.5$ for small values of ℓ, decreasing slowly with increasing ℓ due to the decrease in the magnetic field strength.

e. Finally, the linear density of photons over $\Delta\ell$ is calculated, and the integration is continued until this density falls below a preset value.

With the above information we have proceeded to calculate the response of a detector to determine the specific characteristics of a detector.

4. RESPONSE OF A DETECTOR

It can be noticed from Figure 4a that, when an electron passes through the detector, all the photons would be incident only on the convex side of the trajectory along a straight line. This is indeed a special situation and makes the identification of the electron event very unique. If the electron does not intercept the detector, one can still make use of the property that the incident photons are collinear in the detector to detect electrons. The number of photons required to identify an event unambiguously is $n_\gamma = 3$. However, depending upon the resolution of the detector, one may need a different criterion with $n_\gamma > 3$. This criterion sets constraints on the size and spatial resolution of the detector. Therefore, we examine in some detail the response of a detector as a function of energy for different values of n_γ and for various detector sizes.

In order to investigate the response of a detector, we define the response area A_R of an instrument as the area in the plane of the detector, in which the instrument detects at least n_γ photons emitted by the electron arriving within this area. By virtue of this definition, it is clear that A_R is not the same as the detector area A, but could be smaller or larger. The following properties of A_R can be inferred from the theory of synchrotron radiation and from Figure 4a, in which one notices that the linear density of photon on the detector plane decreases as the distance ℓ from the electron increases.

a. As the value of n_γ increases, one requires the detector to be close to the incident electron and hence, A_R decreases with increasing n_γ.

b. The bigger the detector, the higher is the number of photons detected even if the detector is kept at a large distance from the electron, and therefore A_R increases with A.

c. The mean number of photons emitted by an electron is proportional to $B_\perp$, while the radius of curvature is inversely proportional to $B_\perp$. As a result, the linear density of photons emitted (Figure 4a) is independent of $B_\perp$. As the displacement ℓ of the electron increases with $B_\perp$, A_R increases with $B_\perp$ hence depends on the arrival direction of electron (Z,ϕ).

d. As the energy of the electron increases, the curvature decreases and the linear density of photon increases. This enables higher energy electrons to be detected even at large ℓ from the detector, and hence A_R depends upon E_0.

e. The photon spectrum decreases exponentially above E_c (Figure 1). Therefore, for an instrument with a threshold energy for detecting photons, A_R would decrease to zero rapidly below a critical low value of E_0, at which the threshold energy becomes larger than E_c.

From the above, it is clear that A_R is a function of A, n_γ, Z,ϕ, and E_0. In order to evaluate these dependences quantitatively, we have made use of a circular detector so that the circular symmetry eliminates the influence of shape. As shown in Figure 4b, the detector is divided into a number of strips of width Δb parallel to the plane of curvature of the electron. Let the length of one such strip be L and n_γ = 3. If the electron arrives at O, it would have 3 photons (filled circles) associated with it to be detected by the instrument between O and D. Since no photons would be incident on the concave side of the trajectory, part of the detector stip OA does not record any photon. Therefore, the minimum length required by the detector is OD = ℓ_1. The value of ℓ, can be determined from $N_\gamma(< \ell)$ distribution, described in section 3d, by setting $n_\gamma = N_\gamma (< \ell_1)$. As the electron moves towards A, the number of photons detected increases, reaching a value maximum at A, and then decreases. At O' the number of photons recorded by the entire strip is 3 (open circles). The electron arriving beyond O' cannot give rise to 3 photons to be detected and, hence, the maximum distance up to which an electron can be detected is O'D = ℓ_2. The value of ℓ_2 is determined from the relation $n_\gamma = N_\gamma(< \ell_2) - N_\gamma\{< (\ell_2 - L)\}$. The response area of the strip is $(\ell_2 - \ell_1) \times \Delta b$, which is different from the area of the strip. The total response area is the sum of the response area determined for all paralled strips in the direction of ϕ.

We have illustrated in Figure 5 the response pattern of a circular detector of radius 150 cms for electrons arriving at a zenith angle of 45° over Palestine, Texas. Figure 4a is for E_0 = 10 TeV. The detector is shown by thick circles. The thin curves trace the circumference of the response area for n_γ = 5 in the direction of the North, East, and West. The response area towards the South is zero because the magnetic field direction is only

15° from the arrival direction and hence $B_\perp$ is small. The effect of increasing the value of n_γ to 7 photons is shown by the dashed curve for North. The dramatic increase of the response area with E_0 is shown in Figure 5b for E_0 = 20 TeV; here for convenience, this figure is scaled down by a factor of 2. As in Figure 5a, the dotted curve represents the response area of the detector for n_γ = 7. Note that at this energy there is a finite response area in the direction of South, because as E_0 increases, the energy of the photons increases above the threshold set at 20 keV. The following inference can be obtained from this figure: The response area (a) varies with the arrival direction of electrons, (b) appears elongated along the diameter, indicating its dependence on the shape and size of the detector, (c) decreases as the value of n_γ is increased, and (d) increases with energy.

The dependence of A_R on the arrival direction of electrons is shown in the upper part of Figure 6 for the same circular detector and for E_0 = 10 TeV. Curves A, B, C, and D correspond to zenith angles 30°, 45°, 60°, and 75°, respectively for n_γ = 5 photons; curve A' is for n_γ = 7 photons. In the middle part of the figure, we have plotted $B_\perp$ value as a function of the azimuthal angle. One notices a general similarity between these curves and those of A_R. However, the absolute values of A_R at large zenith angles are smaller than at small zenith angles, unlike the values of $B_\perp$. This is due to the fact that the projected area of the detector perpendicular to the direction of electron decreases with cosZ. If one takes this into account, A_R curves would resemble a plot of $(B_\perp - \varepsilon)$ as a function of ϕ, where ε is a constant. Thus one can represent the response area as,

$$A_R(Z, \phi) = a[B_\perp (Z, \phi)\mathrm{Cos}Z - b\mathrm{Cos}^{\alpha}Z]^{\beta} \qquad (9)$$

Here the constants a and b are function of E_0, n_γ, and A; α is approximately a reciprocal of n_γ and is weakly dependent upon E_0, and β is nearly an independent constant. For the example given in Figure 5, the values of the constants are a = 27 m^2, b = 0.122, α = 0.2, and β = 0.75.

In the lower part of Figure 6 we have plotted the mean number of photons > 20 keV emitted by a 10 TeV electron over a path of 10km. These curves resemble the variation of $B_\perp$. Note that the photon emission rate is rather small. Therefore, one needs a sufficiently large area detector for an experimental investigation of high energy electrons, apart from the fact that the flux of these particles is very small.

The response area of a detector as a function of zenith angle is plotted in Figure 7, for various azimuthal angles and for different primary energies. The azimuthal angles chosen in this figure are North, East, Southeast, South, Southwest, and West, which are shown by curves A, B. C, D. E, and F, respectively. The top part of this figure is for primary energy E_0 = 10 TeV, the middle part for 5 TeV and the bottom part for 30 TeV; all these curves are for n_γ = 5 photons for a detector with radius 150 cms. It is clear from this figure that as the primary energy increases, the response area extends to arrival directions at large zenith angles and towards South (low $B_\perp$). It is suggestive from this figure that if one sets zero level for A_R at around 9 m^2 for 30 TeV, the shapes of these modified curves would resemble those of 10 TeV. Similarly a zero-level setting at 6m^2 for 10 TeV would make these curves resemble the 5 TeV curves. These zero-level settings are the result of detector threshold, by which low energy photons emitted by the electron, either due to E_0 being small or due to low $B_\perp$, are not detected. Below 5 TeV, the response area decreases rapidly and becomes negligible even at 4 TeV.

This is an important characteristic of a detector with low energy threshold for photon detection.

We have demonstrated in this section how the response of an instrument depends upon the arrival direction of the electron, the minimum number of photons required to identify an electron event, the active area of the detector, and the energy of the electron. It is clear from our discussions that for a given E_0 there is a threshold area for an instrument, below which it cannot detect electrons. We have also shown that a detector with a low energy threshold for detecting photons, provides a natural threshold energy for electrons. One can take advantage of this property to measure integral flux of electrons. We may also point out that the response area of an instrument depends also on the shape of the detector, as is evident from Figure 5. It can be shown that the response area is larger for a detector elongated in the East-West direction than for a circular detector with the same area. However, the advantage of an elongated detector needs careful study because of the difficulty in design and orientation.

5. ENERGY ESTIMATION OF ELECTRONS

The mean energy of photons emitted by an electron (Equation 7) is proportional to $B_\perp$ and to E_0^2. Therefore, for a given $B_\perp$, the energy of an electron can be determined from the observed mean energy of photons. It is clear from Figure 6 that the value of $B_\perp$ varies with the arrival direction, indicating the necessity of determining the direction of photons. On the other hand, in the X- and γ-ray regime under consideration, it is difficult to build large area detectors, capable of providing directional information with good detection efficiency. However, one also infers from the same figure that the response area increases with the increasing value of $B_\perp$. The latter

observation suggests that the major fraction of the electrons detected by the instrument is dominated by arrival directions with large $B_\perp$ values. This interesting property helps us to examine the viability of using an omnidirectional detector to study cosmic ray electrons.

The number of particles detected by an instrument in a direction (Z, ϕ) is given by

$$N(E_0, Z, \phi)dE_0 = CP(E_0, Z, \phi)tj(E_0)dE_0 \qquad (10)$$

where $j(E_0)$ is the differential energy spectrum of particles, t is the time of observation and CP is the collecting power of the instrument. The collecting power is the product of the projected response area perpendicular to the arrival direction and the solid angle is that direction. Since the number of particles observed is directly proportional to CP, it is possible to draw histograms of the calculated mean energy $\langle E_\gamma \rangle$ using CP. For this purpose, we have divided the zenith angles in to 5° intervals and the azimuth angles into 15° intervals, and calculated for each solid angle bin the values of CP and $\langle E_\gamma \rangle$. Using these values we have constructed histograms of $\langle E_\gamma \rangle$.

We have plotted in Figure 8 histograms of $\langle E_\gamma \rangle$ using an omnidirectional detector of radius 150 cms for E_0 = 10 TeV and n_γ = 5 photons. The distributions marked as A, B, C, and D correspond to arrival directions with zenith angles less than 30°, 45°, 60° and 85°, respectively; they include all azimuthal angles. Because of the finite size of the angular intervals chosen for this purpose these distributions do not look smooth. One notices from this figure that the peak in the distribution shifts to higher energies as one includes larger zenith angles. This is because the mean value of $B_\perp$ over all azimuthal angles is higher for large zenith angles than for small Z (see

Figure 6). A closer examination of Figure 8 reveals that the dispersion about the peak is nearly the same for all distributions. They are asymmetric with half widths at half maximum of about 27 percent of the peak value towards lower energies and about 10 percent towards higher energies. The sharp cutoff in the distribution at higher energies is an important feature because while determining the energy spectrum, it minimizes the spillover from the large flux of low energy electrons to higher energies.

The distributions of mean energy in Figure 8 shows that the energy corresponding to the peak in the distribution depends upon the acceptance angle of the instrument. It is also important to inquire whether this peak energy depends upon other parameters such as n_γ and A. For this purpose we have made use of the calculated collecting powers for zenith angles less than 60°. $\langle E_\gamma \rangle$ distributions for various values of n_γ are shown in Figure 9; the other parameters are kept the same as in Figure 8. The distributions marked as A, B, and C correspond to n_γ values 3, 5, and 7 photons, respectively. It is clear from this figure that the peak value of the energy is the same for all the distributions, suggesting that the peak energy is independent of n_γ. Note that the width of the distribution is also independent of n_γ. A closer examination of this figure reveals that, while the distribution terminates sharply at higher energies for all values of n_γ, it extends to lower energies as n_γ decreases. The former observation is the result of the zenith angle restriction, and the latter is due to the inclusion of low $B_\perp$ directions.

We have shown in Figure 10, the histograms of $\langle E_\gamma \rangle$ for various detector sizes. Histograms marked as A, B, anc C correspond to circular detectors of radii 100 cms, 150 cms, and 200 cms, respectively. We have restricted the zenith angles to < 60° and kept n_γ = 5 photons, so that the histograms C in Figure 8, B in Figure 9, and B in Figure 10 are the same. Figure 10 indicates

that the peak energy as well as the width of the distribution are independent of the area. We also notice that as we increase the area beyond a certain limit, the $\langle E_\gamma \rangle$ does not extend to lower energies. Thus, a comparison between Figures 9 and 10 suggests that the extent of the distribution to lower energies is a sensitive function of n_γ rather than of A.

It is quite evident from the above description that one can determine for a detector, the most probable value of $\langle E_\gamma \rangle$ using the calculated histogram of the type described above. Accordingly, we have estimated for a balloon-borne instrument with 20 keV cutoff, the most probable value of the mean energy $\langle E_\gamma \rangle_m$ at a float altitude of 4 g cm^{-2} of atmospheric depth over Palestine, Texas. A plot of the estimated $\langle E_\gamma \rangle_m$ as a function of the electron energy is shown in Figure 11. It is seen that the calculated data points can be represented by a power law of the type,

$$\langle E_\gamma \rangle_m = 0.0225\ E_o^{1.76}\ \text{MeV} \qquad (11)$$

As inferred earlier, this relationship should be independent of n_γ and A. It can be seen from Figure 11 that at low values of E_o below 5 TeV, the calculated value deviates from the power law as a result of the low energy threshold of the detector and atmospheric absorption of X-rays. The energy dependence obtained here is flatter than the one given in Equation (7). This is because as the energy increases, the detector responds to photons emitted from greater distances from the detector, where the magnetic field is weaker. It is important to mention here that the above relation in Equation (11) is based on the assumption that the instrument has 100 percent efficiency to detect and to measure the energy of photons > 20 keV, without high energy cutoff. In actual practice this is not true, and one needs to obtain a

similar relation by including both the detector efficiency and the energy response.

In an experiment, one makes use of a relation similar to equation (11) to convert the observed mean energy of the photons to electron energy. In the same manner, we have converted the calculated mean energy in each angular bin to electron energy and examined the resultant distribution using the same procedure described earlier. We have plotted in Figure 12, the collecting power as a function of the ratio of the estimated energy to the actual electron energy (E/E_0) in the form of a histogram, for different E_0 values. Histograms marked as A, B, C, and D correspond to electron energies 5 TeV, 10 TeV, 20 TeV, and 50 TeV, respectively. The value of n_γ chosen for this plot is 5 photons and the radius of the detector is 150 cms; no angular restriction is introduced in this plot.

From Figure 12, one infers that except at low primary energies, where the threshold effect narrows the distribution, the rest of the distributions are similar. The apparent spread in the distribution for large primary energies above $E/E_0 \gtrsim 1$ is due to inclusion of large zenith angles as evident from Figure 7. The effect of restricting the zenith angles to $< 70°$ is shown by the dotted line for $E_0 = 50$ TeV. This effect is also noticed in Figure 8, in which the inclusion of angles beyond 60° spread the distribution beyond the peak energy. In an actual instrument, because of the detector depth, there would be zenith angle restriction beyond which the instrument cannot view. It is clear from this figure that for energy estimation, an omnidirectional detector introduces no more than 15 percent dispersion towards under estimating the energy and no more than 5 percent towards over estimating the electron energy.

The major source of uncertainty in determining the energy arises from the fluctuation in the synchrotron emission process. This fluctuation depends upon the value of n_γ chosen; the larger the value of n_γ, the smaller is the fluctuation. The mean number of photons detected would be closer to the value of n_γ for small energies and increases as the electron energy increases. The mean number also depends on the area of the detector. As an example, the mean number of photons at 10 TeV is about 6.8, for $n_\gamma = 5$ and detector radius of 100 cms; this value increases to about 8 as the radius of the detector is increased to 200 cms. At 50 TeV, the corresponding values are about 9.3 and 9.8, respectively. In order to determine the effect of fluctuation one needs to incorporate the detector efficiency and its energy response, and therefore we do not deal with this aspect here.

In the case of a balloon-borne experiment, one may expect that low energy bremsstrahlung radiation by an electron in the residual atmosphere could mix with the synchrotron photons. However, it can be shown that the Landau-Pomeranchuk-Migdal effect (Stanev et al., 1982) sets in around a few hundred MeV, suppressing the emission of low energy photons. On the other hand, the effect of scattering of the electrons could increase the effective response area by a small amount. Although we have taken into account the attenuation of photons by Compton process, it may be mentioned that a small fraction of these scattered photons might arrive at the detector affecting the collinearity, when the minimum n_γ criterion is applied.

6. DETECTION OF ELECTRONS

We have shown that the response area of the detector depends upon the arrival direction, n_γ, E_0 and the active area of the detector. For an instrument with a finite acceptance angle, the collecting power of the

instrument would depend upon n_γ, E_0 and A. The collecting power of the instrument is obtained by integrating $CP(Z,\phi)$ over Z and ϕ. We have plotted in Figure 13, the collecting power of a detector as a function of the active area of the detector for various values of n_γ and E_0. For this purpose we have considered an omnidirectional circular detector of radius R, which is capable of detecting photons of $E_\gamma > 20$ keV, flown over Palestine, Texas at 4 g cm^{-2} of atmospheric depth. Curves A, B, and C correspond to collecting powers calculated using n_γ values of 3, 5, and 7 photons, respectively; the solid curves are for E_0 = 10 TeV and the dashed curves are for E_0 = 100 TeV. One notices that curve C is very much steeper than curve A indicating that the minimum area required to detect electrons of energy 10 TeV using n_γ = 7 photons is about 1.8 m^2; similarly for n_γ = 5 photons, it is about 0.75 m^2. The solid curve A and all the dashed curves are parallel to each other, and they can be represented by a power law of the type proportional to A^α, where α is about 1.43. This is an interesting feature of this technique of detecting electron, in which the collecting power of the instrument has a higher order dependence on the detector area.

The collecting power of this detector is plotted in Figure 14 as a function of the energy of electrons, for various values of n_γ and A. In this figure, curves A, B, and C correspond to different detector sizes with radii 200 cms, 100 cms, and 50 cms, respectively. The solid and dashed curves represent two different selection criteria with n_γ = 3 and 5 photons, respectively. At large values of E_0, these curves become straight lines indicating that the collecting power is proportional to E_0. As the energy decreases, one can recognize the threshold effect of the detector. The collecting power decreases by an order of magnitude as the energy decreases by a factor of 2 soon after it deviates from the linear dependence in energy.

This behavior provides the threshold detection for electrons and, thus, the integral flux can be determined accurately even by a detector with limited energy resolution. It is also evident from this figure and from Figure 13, that the collecting power is very sensitive to both n_γ and A. One infers from this study that, as long as A is not very small and n_γ not very large, the collecting power of a detector is asymptotically proportional to $A^\alpha E_o n_\gamma^\beta$, where $\alpha = 1.43$ and $\beta = -1.8$.

An instrument designed to detect electrons using this technique should be very efficient in detecting photons above 20 keV, because the number of photons emitted by the electron is rather small. This can be achieved by assembling detector elements which respond to different energy intervals efficiently. Proportional counters can be used for X-rays of energy less than 60 keV. These can be followed by NaI or CsI crystals or scintillators to detect photons up to a few MeV, and they are further followed by lead-glass Cherenkov detectors to absorb high energy gamma-rays. Good spatial resolution can be achieved to any desired accuracy in the proportional chambers without difficulty. In the case of other detectors, one can make use of hodoscope techniques (for example, Streitmatter et al., 1981). One needs to make modules of areas less than 50 cms X 50 cms, and they are to be put together to achieve the required total area of the detector. Simultaneous coincidence in more than two such modules would eliminate the vast background of charged particles and reduce the chance coincidence event rates to a minimum level. Apart from a few events due to such chance coincidence, large angle air showers, gamma-ray bursts, and high energy interactions above the detector can trigger the system. The electron event can be unambiguously identified from its unique co-linearity of the observed photons. Time sequence of these

photons can further eliminate any chance coincidence. Such a detector can also be made use of for the study of gamma-ray bursts of short durations.

For an ideal detector of the kind described above, we have calculated the expected rate of electron events by making use of the curves in Figure 7 and a differential energy spectrum of electrons. The recent data on the observed electron spectrum, as summarized by Stephens (1981), can be represented by a power law of the type $j(E_o) \approx 500\ E_o^{-3.2}$ electrons/(m^2 sr s GeV). The event rate thus calculated is shown in Figure 15 as a function of the energy of electron for various values of n_γ and A. Curves A, B, and C in this figure correspond to circular detectors with radii 200 cms, 100 cms, and 50 cms, respectively; the solid and dashed curves relate to values of n_γ = 3 photons and 5 photons, respectively. The collection time in a typical balloon flight is about 20 hours. Using a detector of area $1Cm^2$, a total of about 22 electrons can be observed at energies above 5 TeV using n_γ criterion of 3 photons; this number reduces to about 8.5 for n_γ = 5 photons. From a 14-day space shuttle flight one can collect about 180 events above 5 TeV and about 5 events above 10^{14} eV. As there is no atmospheric absorption of X-rays, the detection threshold is decreased and the number of events would be larger. We have compared these event rates with that expected from a proposed shuttle experiment (Ormes, 1982) as shown by the curve denoted as TRIC. The study of electrons by the TRIC experiment is based on the principle of transition radiation to identify the electron and ionization calorimeter to measure its energy. The expected number of events from this experiment is only 0.5 electron above 5 TeV.

SUMMARY AND DISCUSSIONS

We have shown the viability of detecting electrons above a few TeV using a technique in which the electron can be unambiguously identified by the photons it emits during its traversal in the geomagnetic field. We summarize here some of the important deductions made while examining this technique of detecting ultra high energy cosmic ray electrons.

a. Synchrotron photons are emitted in a narrow cone along the direction of electrons so that they would be incident almost along a straight line on the detector simultaneously. Thus, an electron event can be identified unambiguously by the collinearity and the simultaneity of the photons detected. In addition, if the electron passes through the detector, all these photons would lie only on the convex side of the curvature of the electron, which makes the identification very unique.

b. Most of the photons have energies in the X- and γ-ray regime. Therefore, one requires large area conventional X- and γ-ray detectors with high efficiency for photon detection and spatial resolution good to about a few cms. The same instrument should also be made use of for the study of γ-ray bursts without much modification.

c. Since the mean energy of the photons detected is found to be approximately proportional to the square of the electron energy, one can determine the energy of the electron very accurately. However, the uncertainty resulting from the fluctuations on the emission process depends on the number of photons required to identify the electron. It is also shown that, in order to determine the energy spectrum of electrons accurately over m decades in energy, one needs a detector capable of measuring photons over an energy span of $(m^2 + 2)$ decades.

d. We have demonstrated that the response of a detector is very sensitive to (i) the arrival direction and the energy of the electron, (ii) the number of photons required for the identification of an electron event, and (iii) the area and shape of the detector. Further, it also depends upon the geographic location and the altitude at which the experiment would be performed. Therefore, one needs to carefully evaluate the instrumental response, while designing a large area experiment, after knowing the detector characteristics and the location of the experiment.

e. Though, in principle, one needs to know the arrival direction of an electron in order to determine its energy, we have shown that an omnidirectional detector can be effectively used for the measurement of the electron spectrum. The uncertainty introduced in the energy response, by an omnidirectional detector is asymmetric about the most probable value; the dispersion is about 15 percent towards the lower energies and is about 5 percent towards higher energies. The energy response function of such a detector is found to be independent of (i) the energy of the electron, (ii) the detector area, and (iii) the number of photons required to identify an electron event.

f. An instrument with low energy threshold for detecting photons can be made use of to determine the integral flux of electrons accurately, even with limited energy resolution.

g. An important feature of this technique is that the collecting power of a detector increases with the energy of the electron. This is advantageous for the measurement of electrons, which have a steep energy spectrum. Thus, with this technique, one can cover more energy than with the existing techniques.

h. We have also pointed out the special advantage of large area detectors while using this technique; the collecting power of a detector is proportional to $A^{1.43}$.

From the above discussions, it is quite clear that the detection of electrons using this technique would open up in a new dimension in the study of cosmic ray electrons at energies, where the existing techniques start to fail.

ACKNOWLEDGEMENTS: We express our thanks to Dr. J. F. Ormes for the keen interest and encouragement during this work. We also acknowledge the rewarding discussions with many scientific colleagues.

Note added in proof:

"It was brought to our notice that the possibility of detecting high energy electrons using the synchrotron radiation they emit in the geomagnetic field has been suggested in the past by Prilutskii (1972) and McBreen (1977).

McBreen, B., Possible new methods of detecting cosmic ray electrons by their synchrotron radiation in the geomagnetic field and interstellar field, Proc. 12th ESLAB Symposium, ESA SP-124, 319, 1977.

Prilutskii, O. F., The possibility of registering primary cosmic ray electrons by means of synchrotron radiation in the geomagnetic field, Soviet Phys. JETP Lett., 16, 320, 1972.

REFERENCES

Anand, K. C., R. R. Daniel, and S. A. Stephens, Final results of TIFR cosmic ray electron spectrum in the region 10-800 GeV, Proc. 13th Int. Cosmic Ray Conference, Denver, Vol 1, 355, 1973.

Balasubrahmanyan, V. K. and F. B. McDonald, Cosmic ray experimental observations in 'High energy particles and quanta in astrophysics', ed. F. B. McDonald and C. E. Fichtel, The M.I.T. press, p1, 1974.

Cherry, M. L., Measurements of the spectrum and energy dependence of X-ray transition radiation, Phys. Rev. 17D, 2245, 1978.

Daniel, R. R. and S. A. Stephens, Directional variation of geomagnetic cut-off rigidity around Hyderabad, Proc. Ind. Acad. Sci., 63, See A, 275, 1966.

Finch, H. P. and B. R. Leaton, The Earth's main magnetic field-epoch 1955, Mon. Not. Roy. Astron. Soc., Geophys. Suppl. 7, 314, 1957.

Ginzburg, V. L. and S. I. Syrovatskii, Cosmic magnetobremsstrahlung, Ann. Rev. Astron. Astrophys. 3, 297, 1965.

McCraken, K. A., U. R. Rao, and M. A. Shea, The trajectories of cosmic rays in a high degree simulation of the Earth's magnetic field, M.I.T. Technical Report 77, 1962.

Muller, D. and P. Meyer, The spectrum of galactic electrons with energies between 10 and 900 GeV, Astrophys. J., 186, 841, 1973.

Nishimura, J., M. Fujii, T. Taira, E. Aizu, H. Hiraiwa, T. Kobayashi, K. Niu, I. Ohra, R. L. Golden, T. A. Koss, J. J. Lord, and R. J. Wilkes, Emulsion chamber observations of primary cosmmic ray electron in the energy range 30-1000 GeV, Astrophys. J., 238, 394, 1980.

Ormes, J. F., Cosmic ray composition up to 10^{15} eV: a combination transition radiation and ionization calorimeter detector on Spacelab and a space platform, Proc. Workshop on very high energy cosmic ray interactions, Philadelphia, ed. M. L. Cherry, K. Lande and R. I. Steinberg, p 466, 1982.

Stanev, T., Ch. Vankov, R. E. Streitmatter, R. W. Ellsworth, T. Bowen, Development of ultrahigh-energy electromagnetic cascades in water and lead including the Landau-Pomeranchuk-Migdal effect, Phys. Rev., D25, 1291, 1982.

Stephens, S. A., Propagation of cosmic ray nuclei, electrons and antiprotons, Proc. 17th Int. Cosmic Ray Conf., Paris, Vol. 13, 89, 1981.

Stephens, S. A. and V. K. Balasubrahmanyan, Detection of ultra high energy electrons using Earth's magnetic field as a radiator, Proc. Cosmic Ray Workshop, University of Utah, Ed. T. K. Gaisser, p196, 1983.

Streitmatter, R. E., V. K. Balasubrahmanyan, and J. F. Ormes, Cosmic ray detector for high energy iron nuclei, Proc. 17th Int. Cosmic Ray Conference, Paris, 8, 54, 1981.

Zombeck, M. V., High energy astrophysics handbook, Smithsonian Astrophysical Observatory Special Report No. 386, 1980.

FIGURE CAPTIONS

Figure 1. Energy spectra of synchrotron photons in a magnetic field $B_\perp$ = 0.4G are shown for various electron energies. The solid curves are the differential spectra and the dashed ones are integral spectra.

Figure 2 The normalized angular distributions of photons are shown as a function of θ/ψ, where $\psi = mc^2/E_o$, for various values of E_γ/E_c; these curves are independent of the energy of electron.

Figure 3. Angular distributions of synchrotron photons are shown. Curves A and A' are the differential angular distribution for $B_\perp$ values 0.24G and 0.48G, respectively; curve C is the integral distribution using curve A. Curve B is the differential angular distribution of the energy flow for $B_\perp \simeq 0.24G$.

Figure 4. The upper part of the figure is an exaggerated view of the electron trajectory. B_1A_1, B_2A_2 ... are the tangents at points B_1, B_2... on the trajectory of the electron. The wavy lines indicate the photons, which are intercepted by the detector plane within an angle ϕ. The lower part of the figure is a schematic diagram describing the manner in which the response area of the detector is calculated (see text).

Figure 5. The response pattern of a circular detector of radius 150 cms over Palestine, Texas is shown for an electron arriving at a zenith angle 45° at two different energies, 10 and 20 TeV. The solid thin curves describe the circumference of the response area for n_γ = 5 photons and for different azimuthal directions; the dashed curve is for n_γ = 7 photons. The thick solid curves are

indicative of the detector area; the curves for 20 TeV are scaled down by a factor of two for convenience.

Figure 6. The dependence of the response area (upper part), $B_{\perp}$ (middle part) and the number of photons > 20 keV emitted per 10 km (lower part) are shown as a function of azimuthal angle for different zenith angles. The solid curves are for n_{γ} = 5 photons and the dashed curve for n_{γ} = 7 photons.

Figure 7. The calculated response area is plotted as a function of zenith angle for various azimuth angles as indicated by curves A, B, C, D, E, and F. The upper, middle parts and lower parts of the figure correspond to electron energies of 10 TeV, 5 TeV, and 30 TeV, respectively.

Figure 8. Histograms of the mean energy of the photons as observed by a detector are shown for different zenith angle restrictions for a circular detector of radius 150 cms with E_0 = 10 TeV and n_{γ} = 5 photons. The broken histograms are alternatively used for the sake of clarity in this figure and in the next two figures.

Figure 9. Histograms of mean energy of photons are shown for different n_{γ} values. These histograms include arrival directions up to 60° zenith; the other parameters being the same as in Figure 8.

Figure 10. Histograms of mean photon energy are shown for different circular detectors of radii 100 cms, 150 cms, and 200 cms as indicated; the other parameters being the same as in Figure 8.

Figure 11. The most probable energy obtained from $\langle E_{\gamma} \rangle$ histograms is plotted as a function of the electron energy.

Figure 12. Histograms of the ratio of the estimated energy of electrons using equation (11) to the true energy are shown for an omnidirectional

circular detector of radius 150 cms, with n_γ = 5 photons, for different values of E_0 as indicated. The dashed histogram is for the arrival directions less than 70° zenith.

Figure 13. Collecting power of an omnidirectional detector is plotted as a function of the detector area for different values of n_γ. The solid curves are for E_0 = 10 TeV and the dashed curves are for E_0 = 100 TeV.

Figure 14. Collecting power of an omnidirectional detector is plotted against the energy of electron for circular detectors with different radii. The solid curves are for n_γ = 3 photons and the dashed curves are for n_γ = 5 photons.

Figure 15. The electron event rate expected in a detector is plotted against the electron energy; the symbols used here are the same as in Figure 8. The curve denoted as TRIC is for a proposed experiment in a shuttle using a transition radiation detector and an ionization calorimeter.

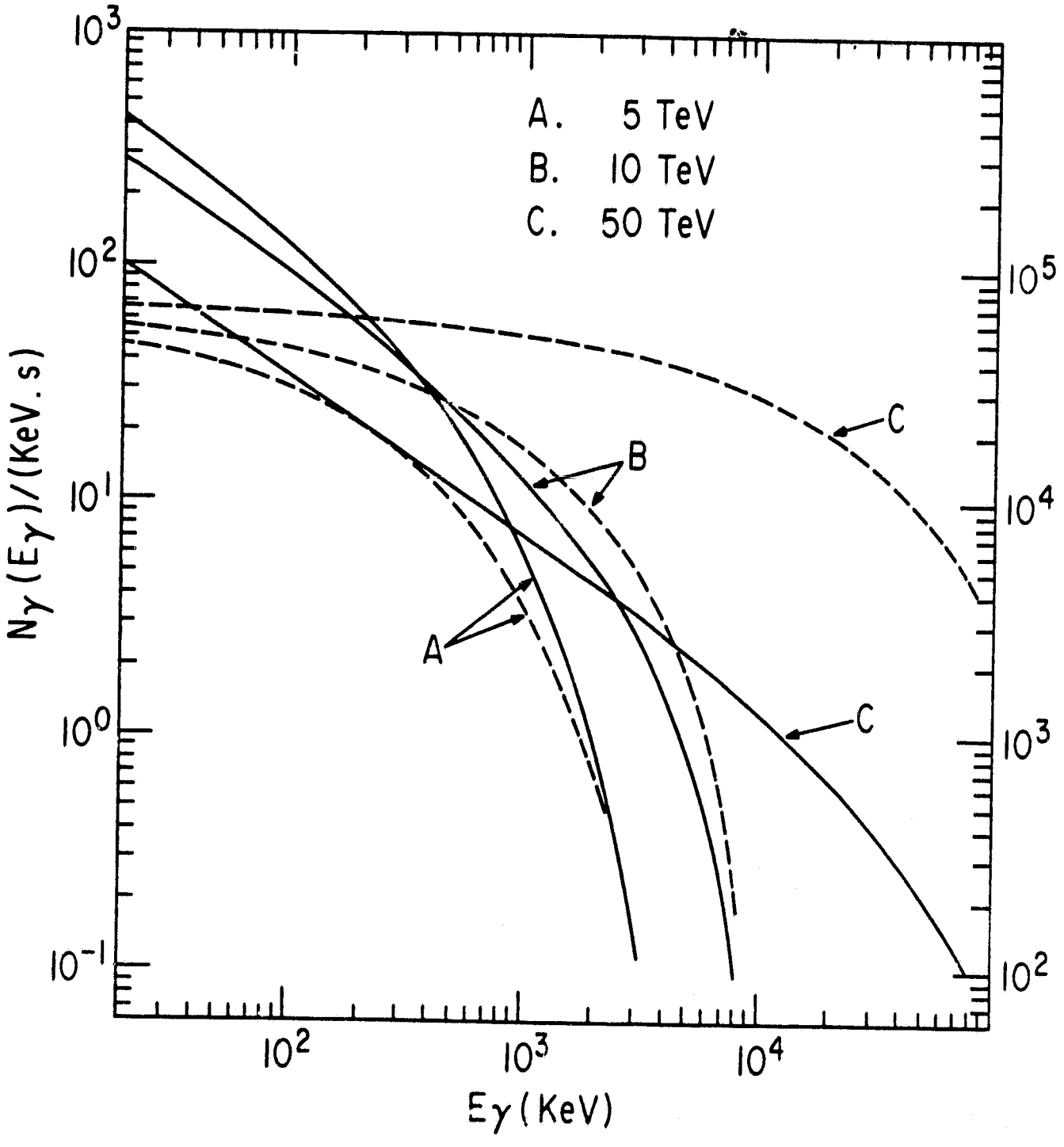

Figure 1

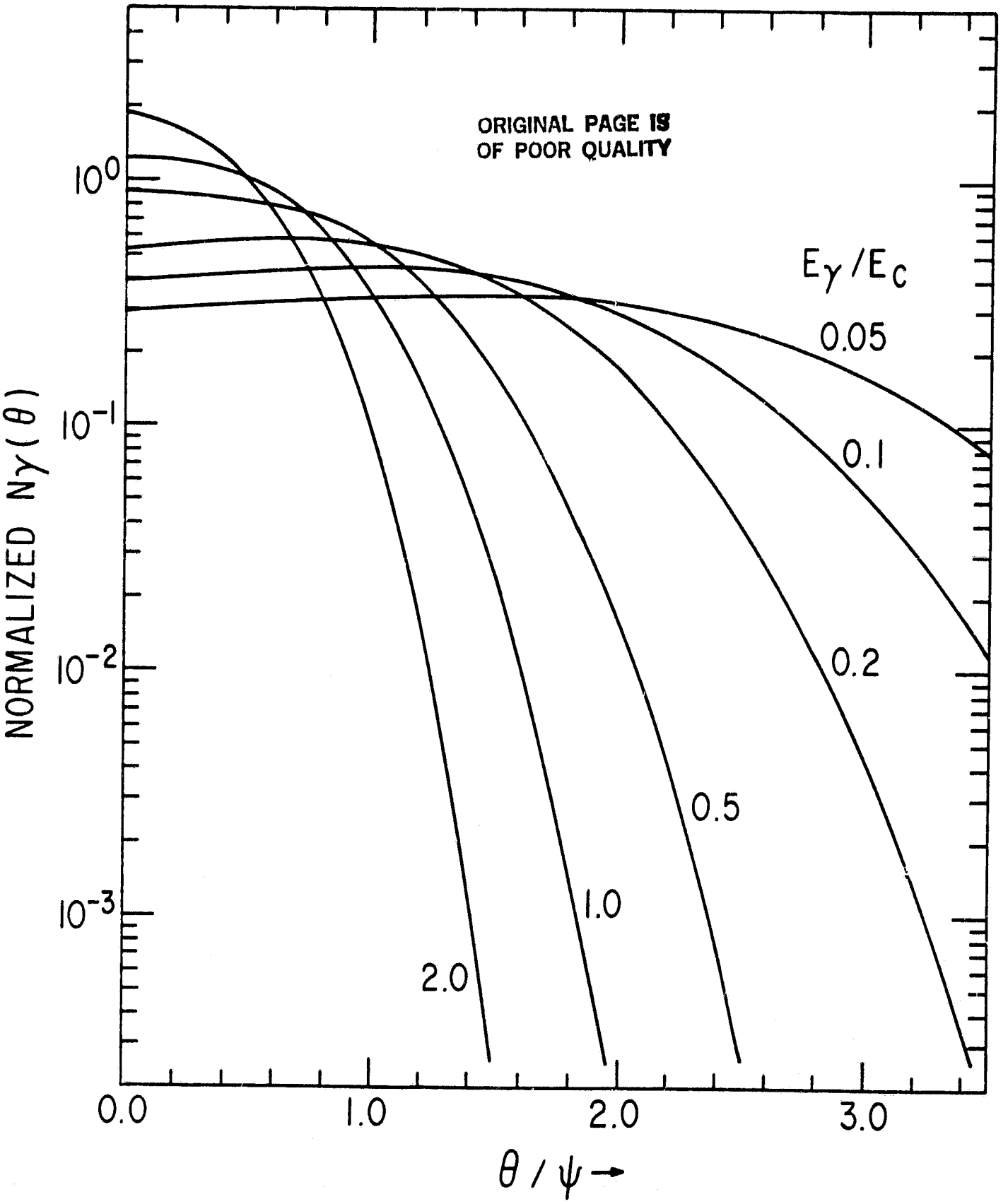
ORIGINAL PAGE IS
OF POOR QUALITY
NORMALIZED Nγ(θ)
10^0
10^-1
10^-2
10^-3
Eγ/Ec
0.05
0.1
0.2
0.5
1.0
2.0
0.0
1.0
2.0
3.0
θ/ψ →

Figure 2

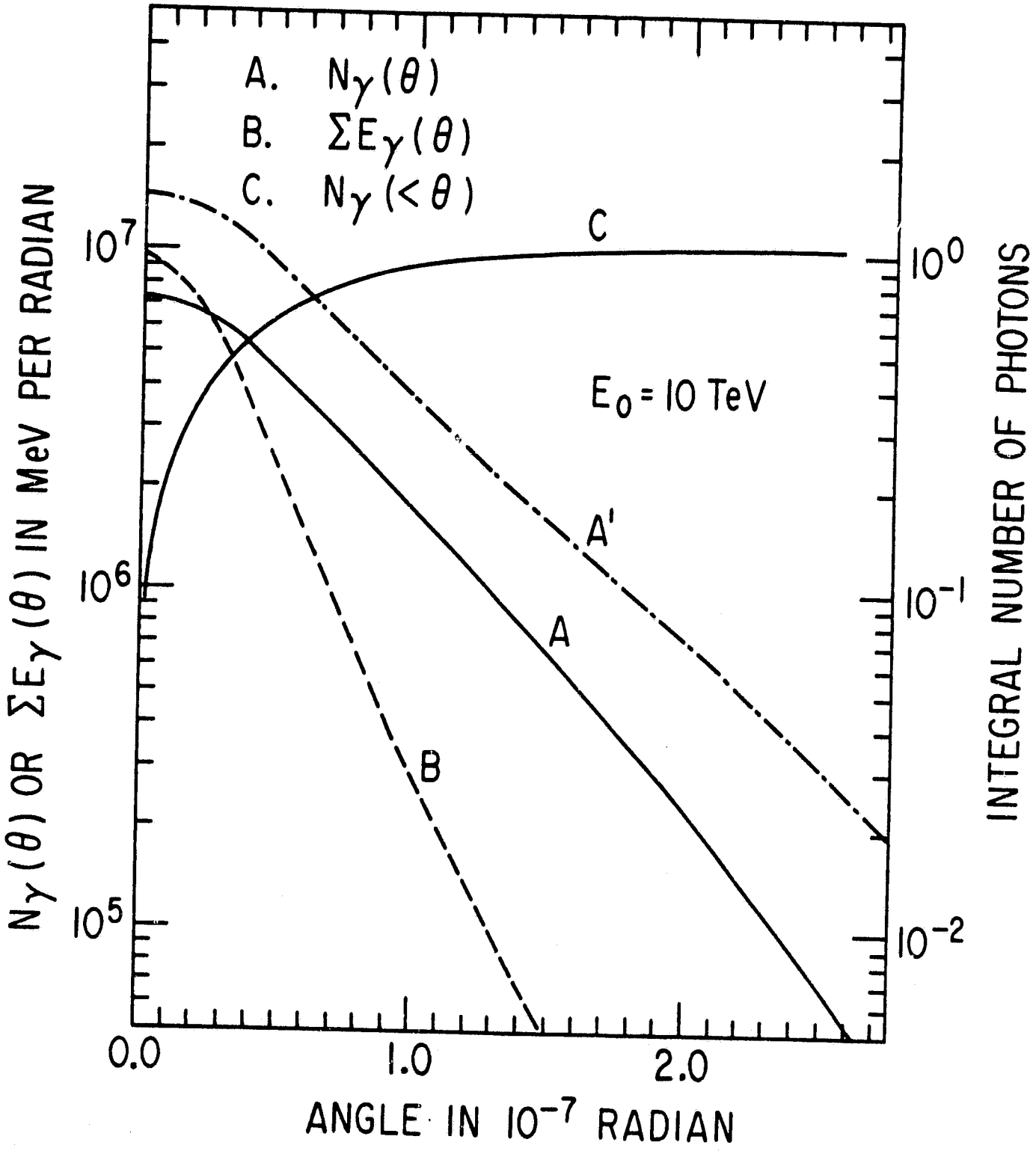

Figure 3

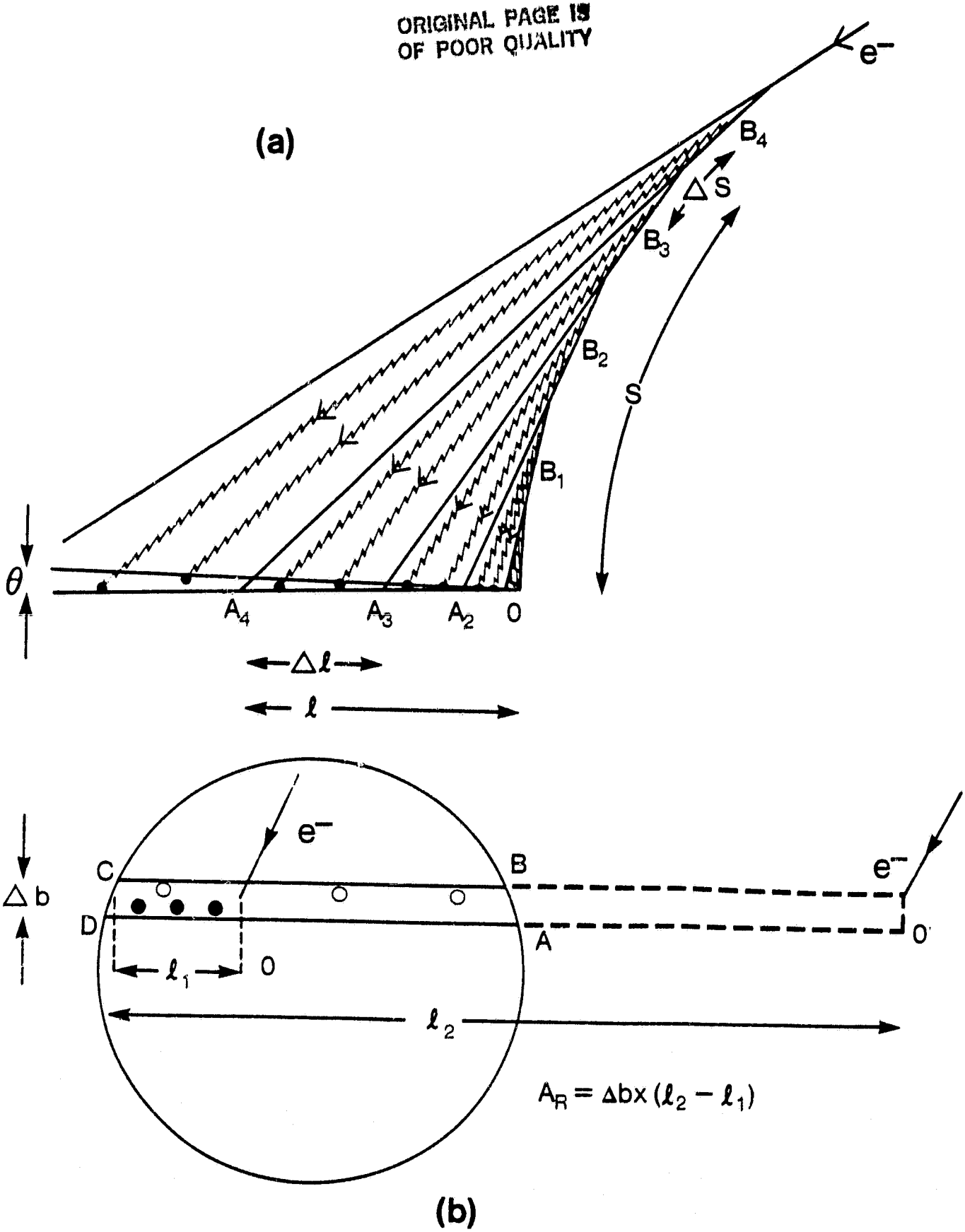

Figure 4

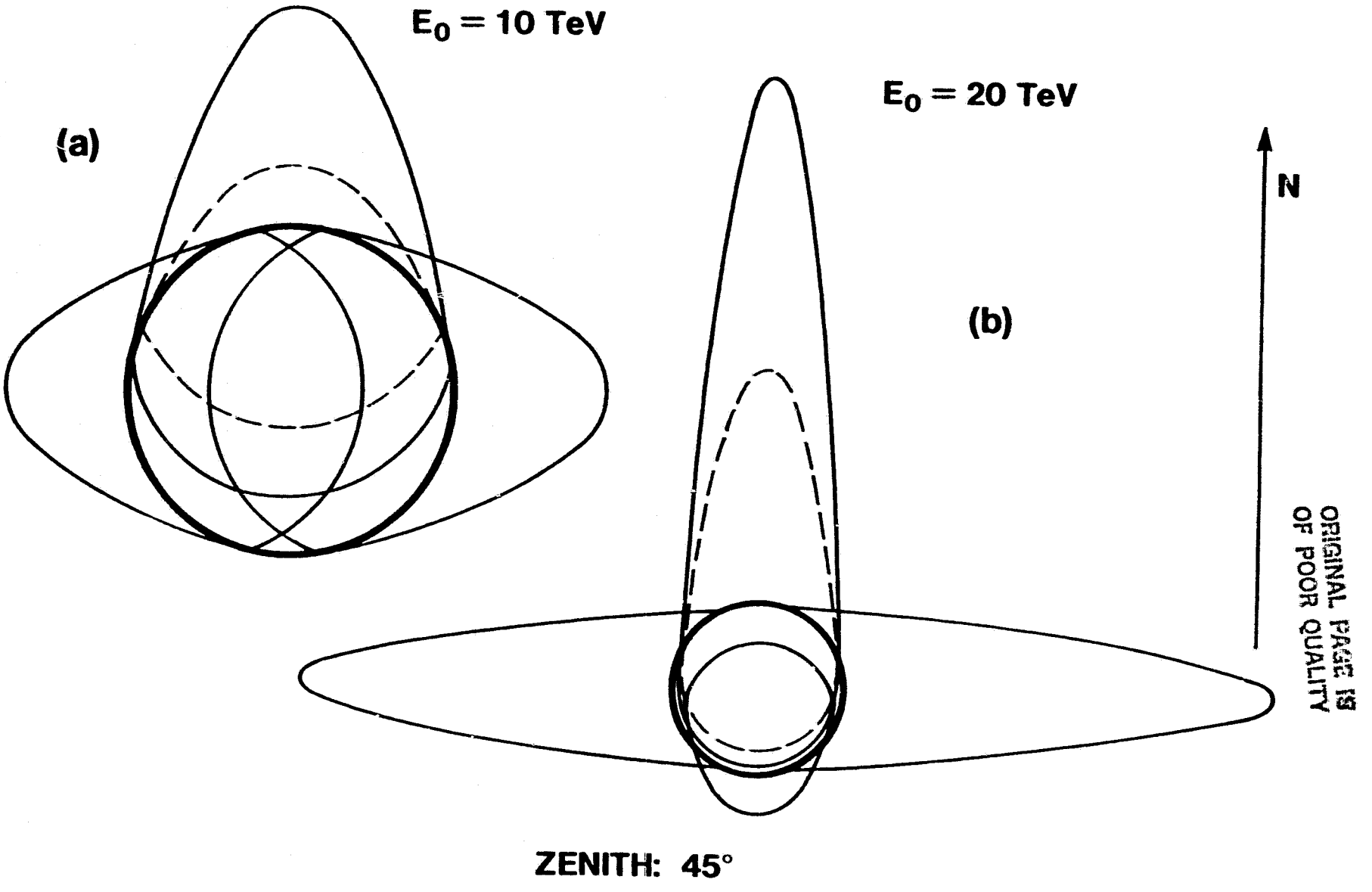

Figure 5

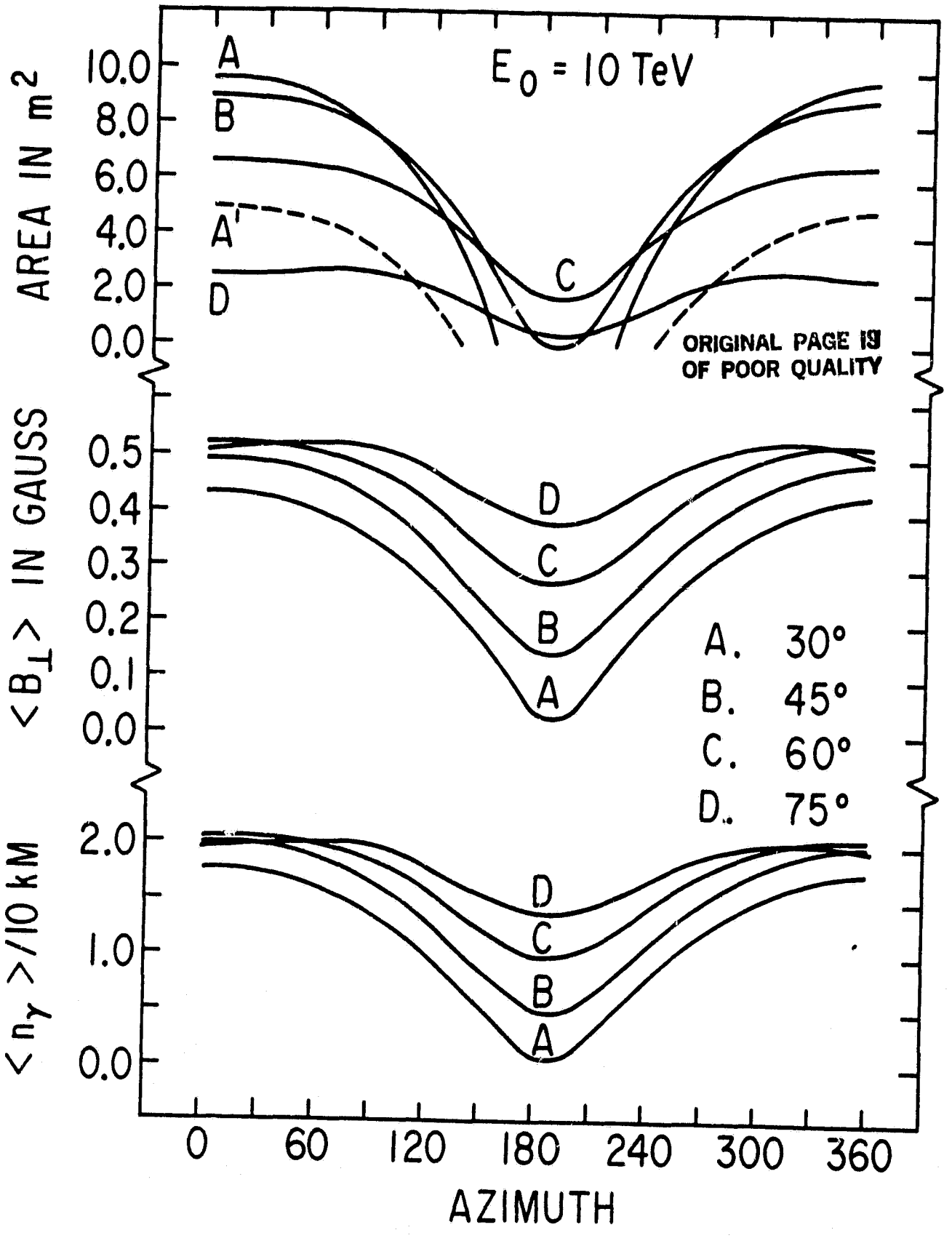
E_0 = 10 TeV
AREA IN m^2
10.0
8.0
6.0
4.0
2.0
0.0
A
B
A'
C
D
ORIGINAL PAGE IS
OF POOR QUALITY
$\langle B_\perp \rangle$ IN GAUSS
0.5
0.4
0.3
0.2
0.1
0.0
D
C
B
A
A. 30°
B. 45°
C. 60°
D. 75°
$\langle n_\gamma \rangle$/10 kM
2.0
1.0
0.0
0
60
120
180
240
300
360
AZIMUTH

Figure 6

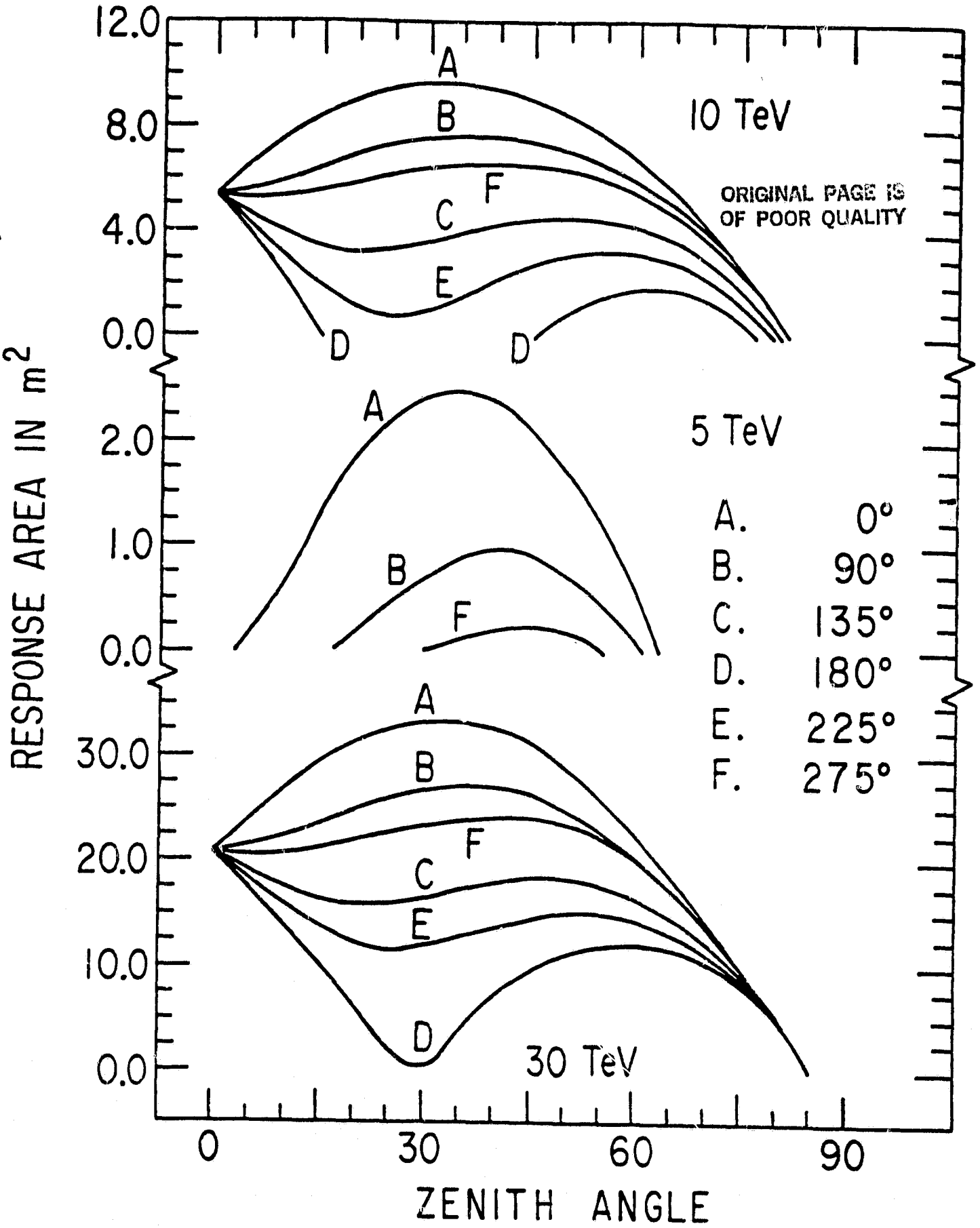
12.0
8.0
4.0
0.0
A
B
F
C
E
D
D
10 TeV
ORIGINAL PAGE IS
OF POOR QUALITY
2.0
1.0
0.0
A
B
F
5 TeV
A. 0°
B. 90°
C. 135°
D. 180°
E. 225°
F. 275°
30.0
20.0
10.0
0.0
A
B
F
C
E
D
30 TeV
RESPONSE AREA IN m²
0
30
60
90
ZENITH ANGLE

Figure 7

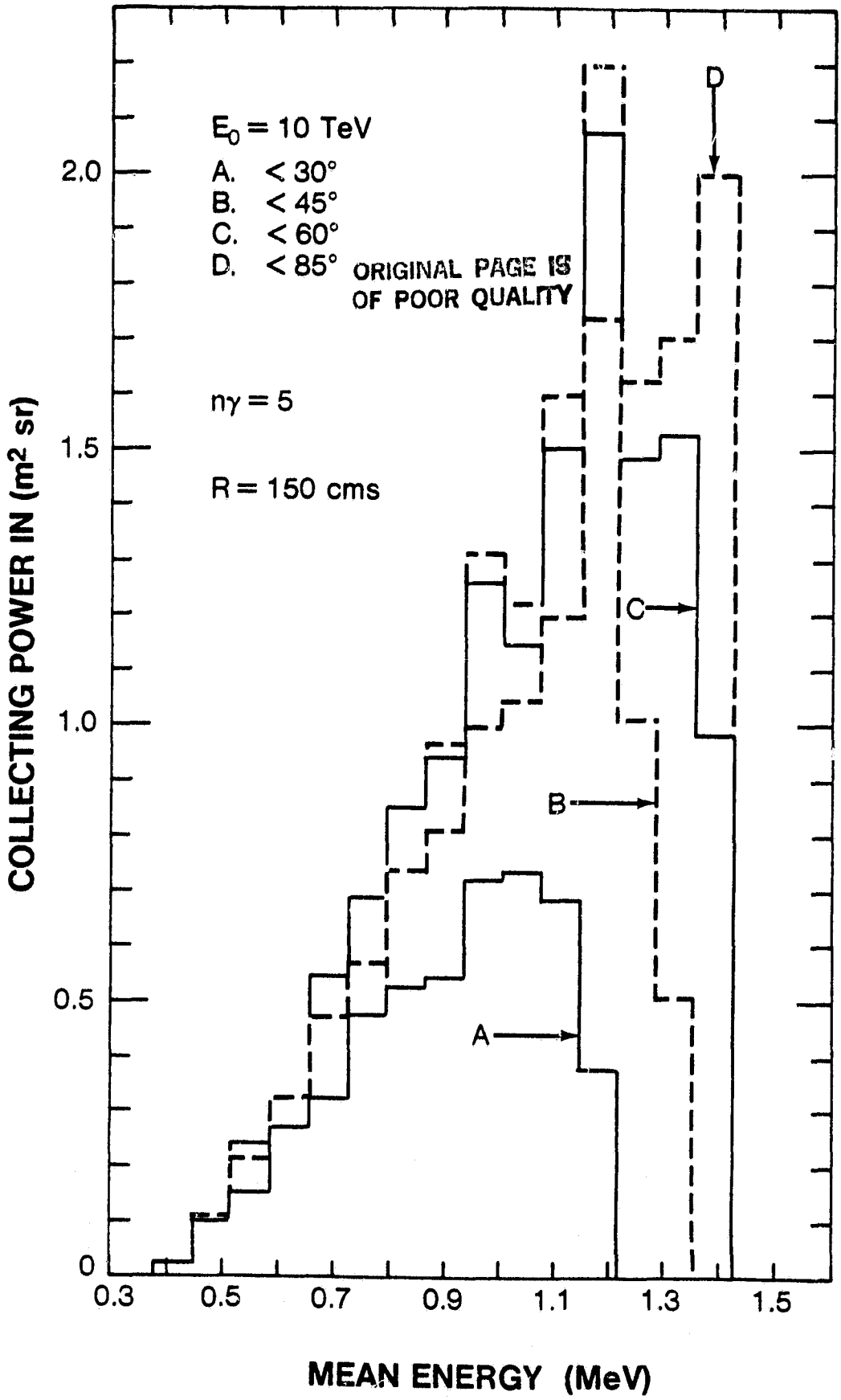
$E_0 = 10$ TeV
A. $< 30°$
B. $< 45°$
C. $< 60°$
D. $< 85°$
ORIGINAL PAGE IS
OF POOR QUALITY
$n\gamma = 5$
R = 150 cms
COLLECTING POWER IN (m^2 sr)
MEAN ENERGY (MeV)
0
0.5
1.0
1.5
2.0
0.3
0.5
0.7
0.9
1.1
1.3
1.5
A
B
C
D

Figure 8

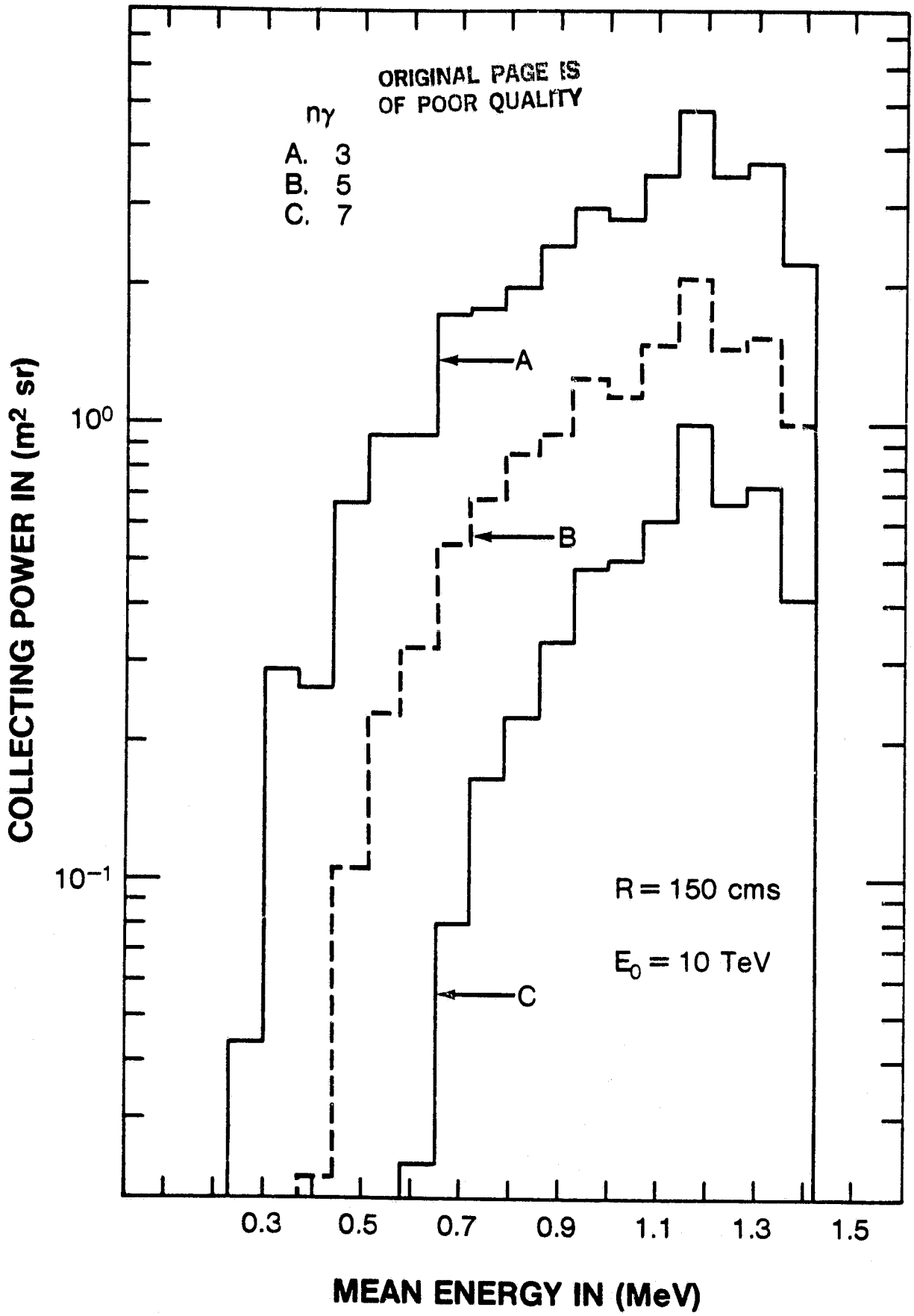
ORIGINAL PAGE IS
OF POOR QUALITY
nγ
A. 3
B. 5
C. 7
A
B
C
R = 150 cms
E0 = 10 TeV
COLLECTING POWER IN (m2 sr)
10^0
10^-1
0.3
0.5
0.7
0.9
1.1
1.3
1.5
MEAN ENERGY IN (MeV)

Figure 9

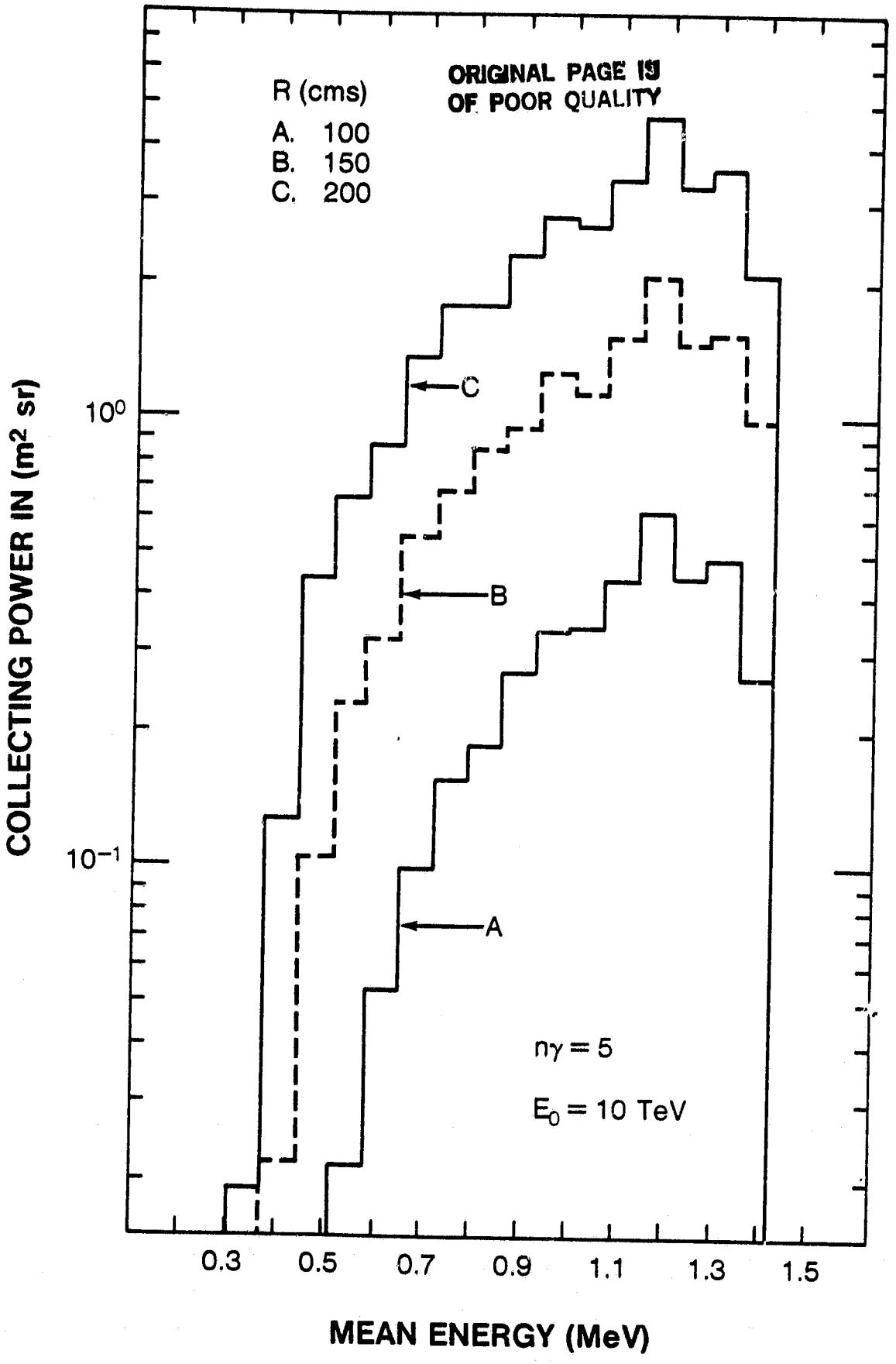
ORIGINAL PAGE IS
OF POOR QUALITY
R (cms)
A. 100
B. 150
C. 200
C
B
A
$n\gamma = 5$
$E_0 = 10$ TeV
COLLECTING POWER IN (m^2 sr)
10^0
10^{-1}
0.3
0.5
0.7
0.9
1.1
1.3
1.5
MEAN ENERGY (MeV)

Figure 10

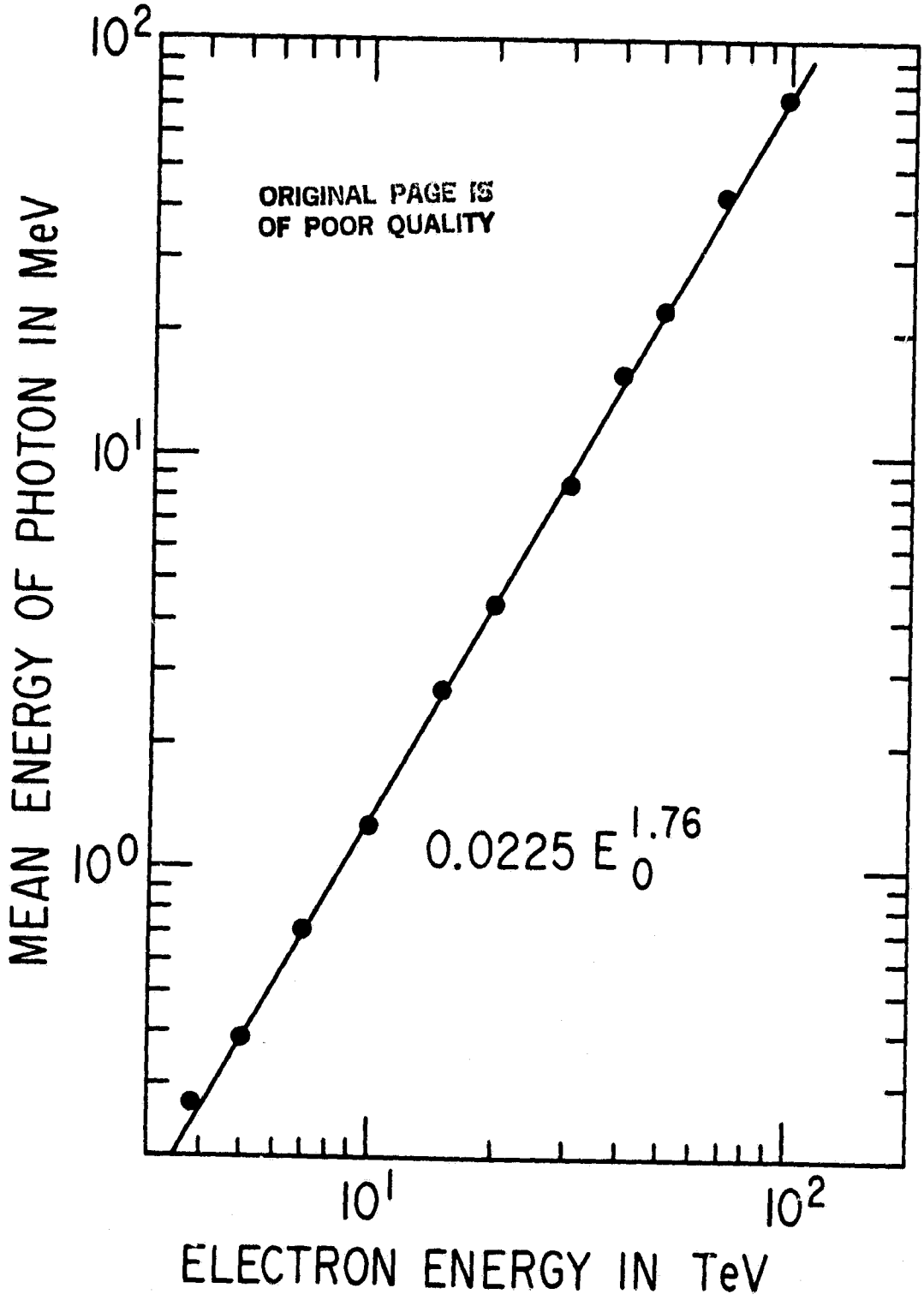
ORIGINAL PAGE IS
OF POOR QUALITY
MEAN ENERGY OF PHOTON IN MeV
ELECTRON ENERGY IN TeV
10^2
10^1
10^0
10^1
10^2
$0.0225\ E_0^{1.76}$

Figure 11

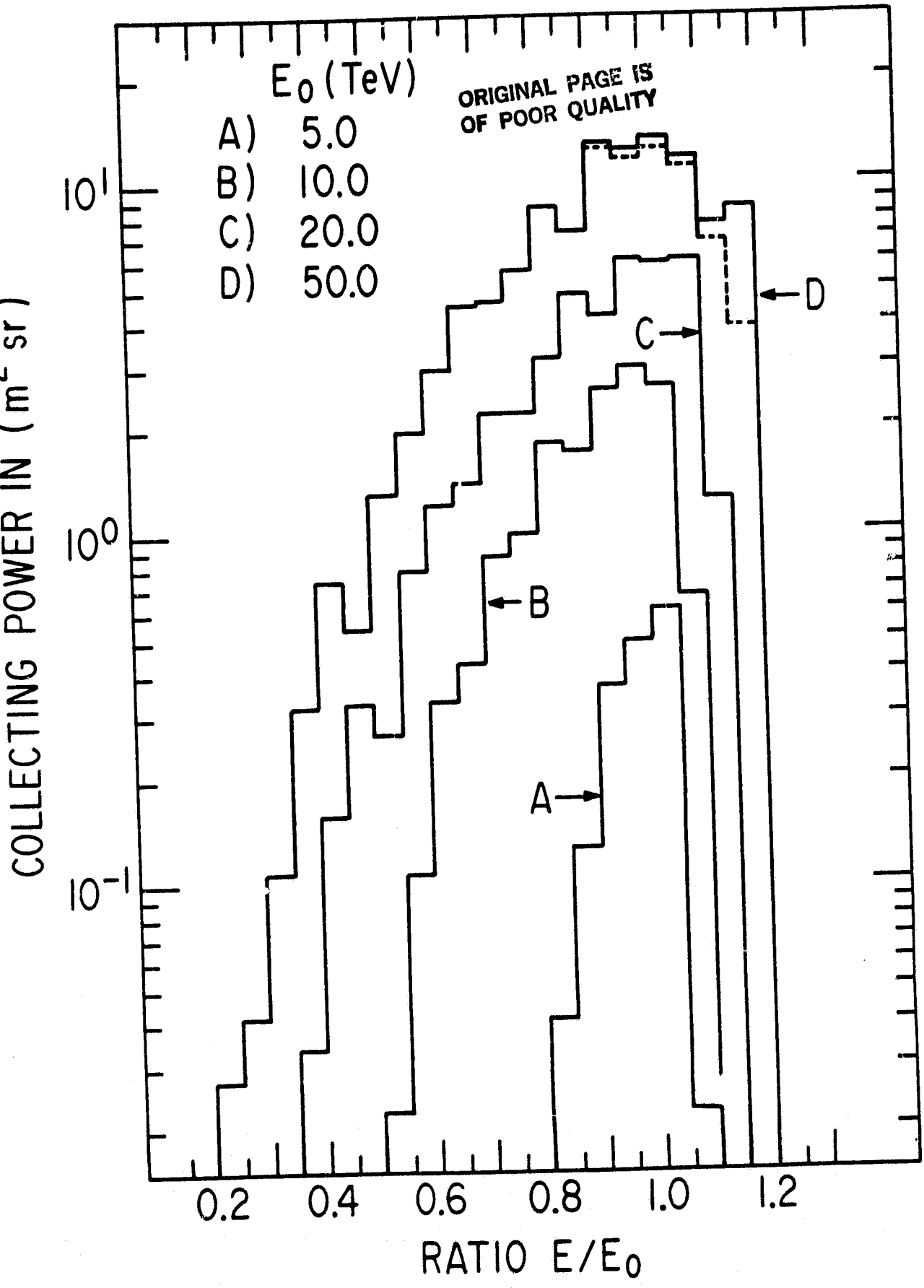
E0 (TeV)
A) 5.0
B) 10.0
C) 20.0
D) 50.0
ORIGINAL PAGE IS
OF POOR QUALITY
COLLECTING POWER IN (m² sr)
10¹
10⁰
10⁻¹
A
B
C
D
0.2
0.4
0.6
0.8
1.0
1.2
RATIO E/E0

Figure 12

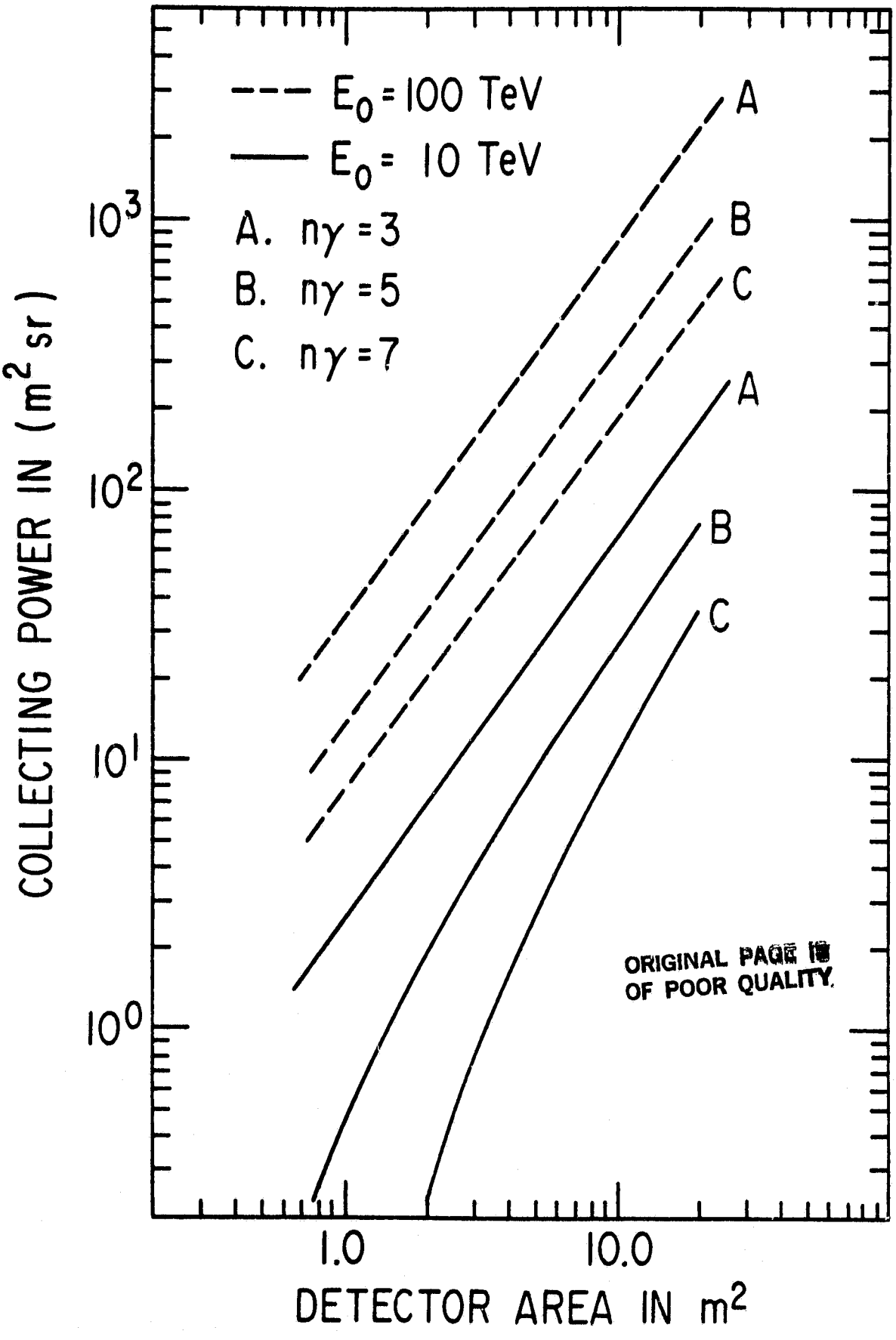
--- E_0 = 100 TeV
—— E_0 = 10 TeV
A. nγ = 3
B. nγ = 5
C. nγ = 7
A
B
C
A
B
C
10^3
10^2
10^1
10^0
COLLECTING POWER IN (m^2 sr)
1.0
10.0
DETECTOR AREA IN m^2
ORIGINAL PAGE IS
OF POOR QUALITY

Figure 13

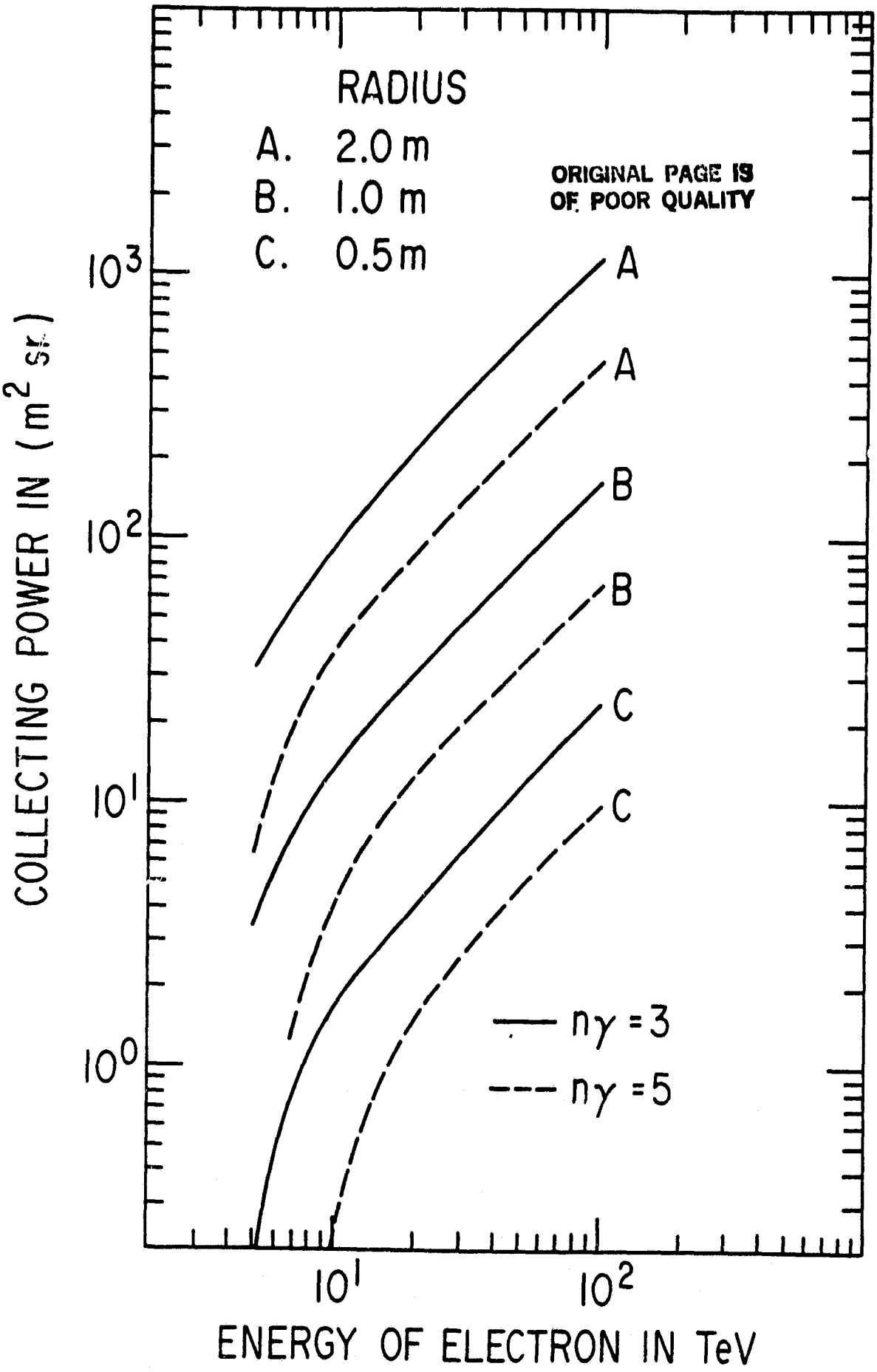
RADIUS
A. 2.0 m
B. 1.0 m
C. 0.5 m
ORIGINAL PAGE IS
OF POOR QUALITY
A
A
B
B
C
C
nγ = 3
nγ = 5
COLLECTING POWER IN (m² sr)
10³
10²
10¹
10⁰
10¹
10²
ENERGY OF ELECTRON IN TeV

Figure 14

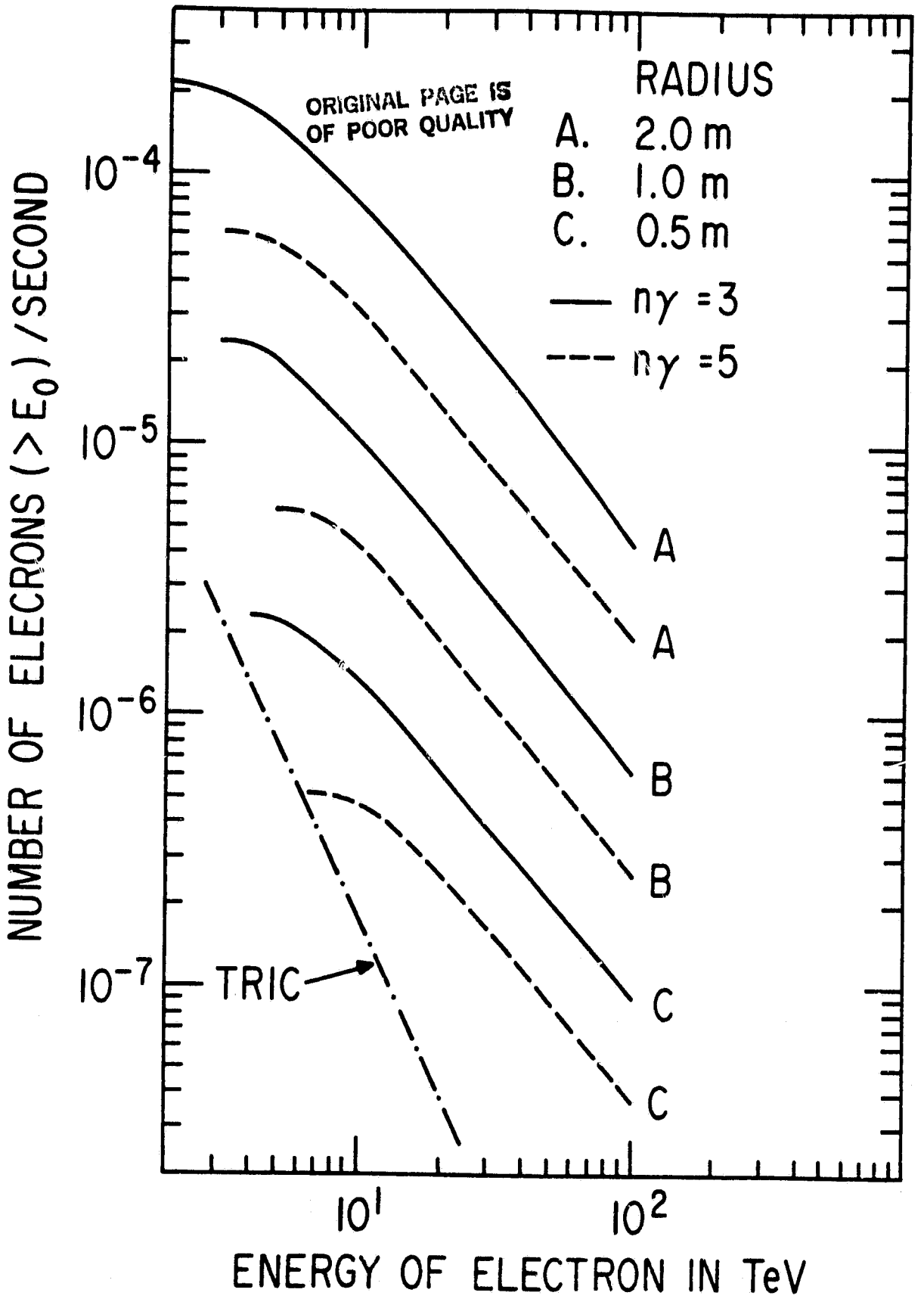
ORIGINAL PAGE IS
OF POOR QUALITY
RADIUS
A. 2.0 m
B. 1.0 m
C. 0.5 m
nγ =3
nγ =5
A
A
B
B
C
C
TRIC
10^{-4}
10^{-5}
10^{-6}
10^{-7}
10^{1}
10^{2}
NUMBER OF ELECRONS (>E_0) /SECOND
ENERGY OF ELECTRON IN TeV

Figure 15